LOS ALAMOS SCIENTIFIC LABORATORY
of the
University of California
LOS ALAMOS • NEW MEXICO

Forward Differential Cross Sections for the Reaction $p + p \rightarrow d + \pi^+$ in the Range 3.4 to 12.3 GeV/c

UNITED STATES
ATOMIC ENERGY COMMISSION
CONTRACT W-7405-ENG. 36

LA-4483-MS
SPECIAL DISTRIBUTION

LOS ALAMOS SCIENTIFIC LABORATORY
of the
University of California
LOS ALAMOS • NEW MEXICO

Forward Differential Cross Sections for the Reaction $p + p \rightarrow d + \pi^+$ in the Range 3.4 to 12.3 GeV/c

This report was printed by the University of Chicago; courtesy copies have been supplied to Los Alamos Scientific Laboratory for issuance as an LA...MS report.

FORWARD DIFFERENTIAL CROSS SECTIONS FOR THE REACTION $p + p \rightarrow d + \pi^+$ IN THE RANGE 3.4 to 12.3 GeV/c*

H.L. Anderson, M.S. Dixit, H.J. Evans, K.A. Klare,
D.A. Larson, and M.V. Sherbrook
University of Chicago

R.L. Martin
Argonne National Laboratory

D. Kessler
Carleton University, Ottawa

D.E. Nagle and H.A. Thiessen
University of California, Los Alamos Scientific Laboratory

C.K. Hargrove and E.P. Hincks†
National Research Council of Canada, Ottawa

and

S. Fukui
Nagoya University, Japan

*Research supported by the National Science Foundation, the U.S. Atomic Energy Commission, and the National Research Council of Canada. Submitted by M.V. Sherbrook to the Department of Physics, The University of Chicago, in partial fulfillment of the requirements for the Ph.D. degree.

†Also at Carleton University, Ottawa, Canada.

ACKNOWLEDGEMENTS

It is a pleasure to acknowledge the contributions of R.L. Armstrong, G. Black, R.R. Gabriel, C.L. Hung, J.P. Legault, J.W. Lillberg, J.G. Michelassi, P.A. Plowe, J. Redfern, R.A. Ryan, and R.B. Wilberg in the construction of the apparatus and the running of the experiment, and the help of V. Stovall and A. LaRotonda in the data reduction.

We wish to thank Drs. G.J. Igo and K.W. Edwards for their help in the early stages of the experiment. Dr. R.R. Silbar helped us anticipate what results we might expect. Dr. E.P. Steinberg gave us important advice about the measurement of the beam intensity and put his equipment for this purpose at our disposal. One of us (EPH) wishes to thank Prof. R.D. Barton for helpful discussions regarding the time-of-flight instrumentation. In addition, HLA wishes to thank Profs. G. Wentzel and Y. Nambu for useful discussions of the results.

We appreciated the help of various members of the Argonne ZGS staff. In particular, C.W. Testin gave invaluable assistance with the alignment of our spark chambers, A.R. Passi helped with the installation of our

equipment on the ZGS floor, and R.J. Lari measured the effective length of the bending magnets. Other members of the ZGS staff contributed in the competent operation of the accelerator and auxiliary equipment.

TABLE OF CONTENTS

LIST OF TABLES

LIST OF ILLUSTRATIONS

ABSTRACT

A missing-mass spectrometer, employing optical spark chambers with automatic vidicon readout, was used to measure the forward differential cross section ($\cos\theta_{c.m.} \approx 0.995$) for the reaction $p + p \rightarrow d + \pi^+$ at closely spaced settings of the incident proton momentum in the range $p_o = 3.4$ to 12.3 GeV/c. The deuterons from the reaction were identified by time-of-flight, and their momentum and angle of emission measured by a reconstruction of the spark chamber tracks. Since the incoming proton momentum was accurately known, the missing-mass associated with deuteron production could be deduced. Single pion production was identified by the appearance of a clear peak in the plot of missing-mass at the pion mass.

The data confirm the existence of a prominent peak in the forward cross section at $E_{c.m.} = 3.0$ GeV and show a hitherto unreported shoulder at $E_{c.m.} = 3.7$ GeV. This structure, along with the well known sharp maximum at $E_{c.m.} = 2.2$ GeV may be understood on the basis of a one-pion-exchange model as reflecting the behavior of the $T = 3/2$ isobars in the pion-nucleon scattering. Above $E_{c.m.} = 3.9$ GeV, the cross section decreases monotonically as the -2.5 power of the square of the total c.m. energy, s.

This feature reflects the behavior of the πp scattering cross section. The structureless upper energy region can be accommodated within the framework of Regge theory. The cross section $d\sigma/du$ extrapolated to $u = 0$ varies as the -3.2 power of s, midway between that expected for N_α and N_γ trajectories.

CHAPTER I

INTRODUCTION

In the course of a general survey of bosons produced in high energy p-p collisions, an extensive set of forward differential cross sections was measured for the reaction

$$p + p \rightarrow d + \pi^+ \qquad (1)$$

over a range of incident momenta from 3.4 to 12.3 GeV/c. In this report we describe this aspect of the work and present a detailed description of the apparatus and the measurements, together with what can be said of the significance of the results. A brief report has already been published.[1]

The general motivation of our work was to use the observation of the production of a deuteron as a device for determining the fate of the two nucleons of the initial state. Since the initial two proton state has isospin T = 1 and the deuteron has T = 0, whatever else is produced must

---

[1] H.L. Anderson, M.S. Dixit, H.J. Evans, K.A. Klare, D.A. Larson, M.V. Sherbrook, R.L. Martin, K.W. Edwards, D. Kessler, D.E. Nagle, H.A. Thiessen, C.K. Hargrove, E.P. Hincks, and S. Fukui, Phys. Rev. Letters 21, 853 (1968).

have total isopin T = 1 and have baryon number B = 0. The pion is the simplest object with these quantum numbers and turned out to be easy to identify by the missing-mass technique. By knowing the momentum and direction of the incoming proton and by measuring precisely the momentum and angle of the emergent deuteron, we could deduce the missing-mass of whatever else was produced. Single pion production could be identified because of the appearance of a clear peak, generally with low background, at the pion mass position in a missing-mass plot.

Reaction (1) has particular importance in high energy physics because it is one of the few two body reactions which is experimentally accessible in direct, inverse, as well as in the crossed channels. It thus provides an opportunity to test the theorems that govern the relationships among these channels. Early measurements at low energies[2] used the comparison of the direct and inverse channels and the principle of detailed balance to establish that the spin of the pion is 0.

When we began our measurements very few measurements had been made above 3.6 GeV/c incident proton momentum. On the other hand, a relatively rich literature dealt with the

---

[2] R. Durbin, H. Loar, and J. Steinberger, Phys. Rev. 83, 646 (1951); D. L. Clark, A. Roberts, and R. Wilson, Phys. Rev. 83, 649 (1951); W. F. Cartwright, C. Richman, M. N. Whitehead, and H. A. Wilcox, Phys. Rev. 91, 677 (1953).

measurements and their interpretation below this. A reasonably satisfactory account of the very low energy behavior had been provided by the phenomonological analysis of Rosenfeld,[3] and Gell-Mann and Watson.[4] However, this was suitable only when few angular momentum states were involved. The resonant behavior that appeared at 660 MeV proton energy was analyzed by Mandelstam[5] in terms of what we might today refer to as a direct channel resonance in which the pion and one of the nucleons are in a (3/2, 3/2) isobar state, and this in turn is in an S-state interaction with the second nucleon. Such a state, with angular momentum $J = 2$, which is fed from a $^1D_2$ diproton initial state, gives a plausible if not entirely satisfactory account of the peak at 2.17 GeV c.m. energy.

The Mandelstam approach owes its success to the small number of angular momentum states which can contribute in the low energy region. More detailed measurements of the reaction in this energy region recently obtained by Richard-Serre[6] have shown the inadequacies of the Mandelstam approach and the importance of higher angular momentum states.

---

[3] A. H. Rosenfeld, Phys. Rev. 96, 139 (1954).

[4] M. Gell-Mann and K. M. Watson, Ann. Rev. Nucl. Sci. 4, 219 (1954).

[5] S. Mandelstam, Proc. Roy. Soc. (London) A244, 491 (1958).

[6] C. Richard-Serre, CERN Report 68-40 (unpublished).

When measurements at somewhat higher energy were carried out[7-11] the popular approach was to analyze the data in terms of one-pion-exchange (OPE) and one-nucleon-exchange (ONE) models. In the work of Heinz et al.[9] in the energy region between 1 and 2.8 GeV neither model proved quantitatively satisfactory, but the qualitative behavior of the one-nucleon-exchange model led these authors to conclude that the one-nucleon-exchange process could conceivably be the dominant mechanism, and with suitable refinements, the model could give better quantitative agreement with the experiment.

Such a conclusion seems unjustified in view of the marked resonance behavior which was evident just below 1 GeV, since one-nucleon-exchange provides no mechanism for such behavior. It is difficult to see how refinements in the model alone could help resolve this situation. On the

---

[7]K. R. Chapman, T. W. Jones, Q. H. Khan, J. S. C. McKee, H. B. Van Der Raay, and Y. Tanimura, Phys. Letters, 253 (1964).

[8]D. Dekkers, B. Jordan, R. Mermod, C. C. Ting, G. Weber, T. R. Willitts, K. Winter, X. De Bouard, and M. Vivargent, Phys. Letters 11, 161 (1964).

[9]R. M. Heinz, O. E. Overseth, D. E. Pellet, and M. L. Perl, Phys. Rev. 167, 1232 (1968).

[10]F. Turkot, G. B. Collins, and T. Fujii, Phys. Rev. Letters 11, 474 (1963).

[11]G. Cocconi, E. Lillethun, J. P. Scanlon, C. A. Ståhlbrandt, C. C. Ting, J. Walters, and A. M. Wetherell, Phys. Letters 7, 222 (1963).

other hand, it was pointed out to us by Silbar,[12] on the basis of a one-pion-exchange model, that a rich structure could be expected at higher energies because of the influence of the resonances that show up in the πp scattering. This helped motivate the present work.

Here, and more generally, with only primitive theoretical tools available there are a variety of possible models which provide some amount of plausibility from seemingly quite different points of view. It isn't even clear that it is a matter of choice among them. The duality argument[13] suggests that different models may represent equivalent ways of describing the same thing. To help clarify the situation, there is a need for more detailed data over a wider range of the observable parameters. We present here a substantial addition to the data available in the range 3.4 - 12.3 GeV/c incident momentum where previously only a few measurements were available.

The forward differential cross section for reaction (1) was measured in this experiment at 29 settings of the incident proton laboratory momentum in the range p_o = 3.4 to 12.3 GeV/c. The deuteron spectrometer, employing optical spark chambers with an automatic vidicon readout, was used to determine the deuteron momentum and angle of emission.

---

[12] R. Silbar, private communication.

[13] C. Schmid, Phys. Rev. Letters 20, 689 (1968).

The laboratory production angle of the deuterons was held fixed at 5^{o} with respect to the incident proton beam. We detected the deuterons emitted backward in the center-of-mass system, but due to the symmetry of the initial state of reaction (1), no distinction need be made between positive and negative values of $\cos\theta_{c.m.}$. The $\cos\theta_{c.m.}$ was nearly constant varying from 0.9928 at the lowest incident momentum to 0.9985 at the highest. The laboratory momentum of the backward deuterons covered the range p_d = 1.14 to 1.34 GeV/c. The transverse momentum was small varying from 0.099 to 0.116 GeV/c. The total c.m. energy covered the range $E_{c.m.}$ = 2.9 to 5.0 GeV.

CHAPTER II

EXPERIMENTAL TECHNIQUE

In the missing-mass method used in this experiment, no attempt was made to observe the pion of reaction (1). Rather, its presence was inferred from energy-momentum conservation using the known momentum of the incoming proton and the measured momentum and angle of the emergent deuteron. Figure 1 is a diagram of a general collision process with incoming particles 1 and 2 and outgoing particles 3 and X where X represents all particles in the final state other than particle 3. We shall take particles 1 and 2 to be protons and particle 3 to be a deuteron. Energy and momentum conservation imply that $p_1 + p_2 = p_3 + p_X$ where p_1, p_2, and p_3 are the four-momenta of particles 1, 2, and 3 and p_X is the remaining four-momentum in the final state not accounted for by particle 3. Solving for the Lorentz invariant scalar p_X^2, which we call the missing-mass squared MM^2, we obtain in terms of the laboratory coordinates

$$MM^2 = 2m^2 + M^2 + 2m\,(p_o^2 + m^2)^{1/2} - 2(p_d^2 + M^2)^{1/2}$$

$$\times\,[(p_o^2 + m^2)^{1/2} + m\,] + 2p_o p_d \cos\theta_d$$

Fig. 1.--General collision process with two incoming particles having four-momenta p_1 and p_2 and X + 1 outgoing particles having four-momenta p_3 and p_X where X stands for all particles in the final state other than particle 3.

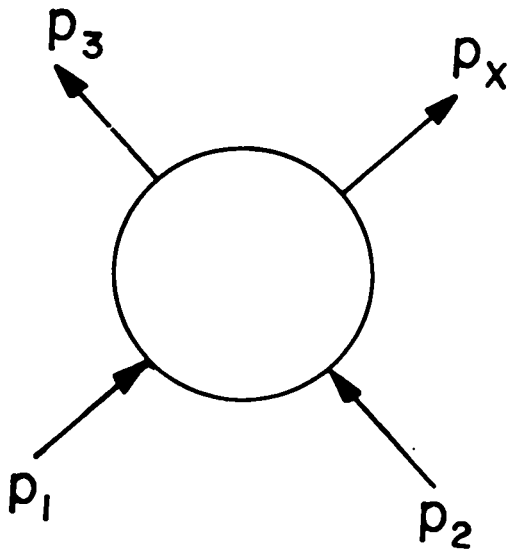

Fig. 1.

Fig. 2.--Kinematics diagram for the reaction $p + p \rightarrow d + \pi^+$ expressed in terms of the deuteron laboratory momentum p_d and angle θ_d. The solid curve corresponds to the minimum incident proton momentum observed $p_o = 3.4$ GeV/c and the dashed curve to the maximum $p_o = 12.3$ GeV/c. The region studied corresponds to deuterons moving backward in the c.m. system.

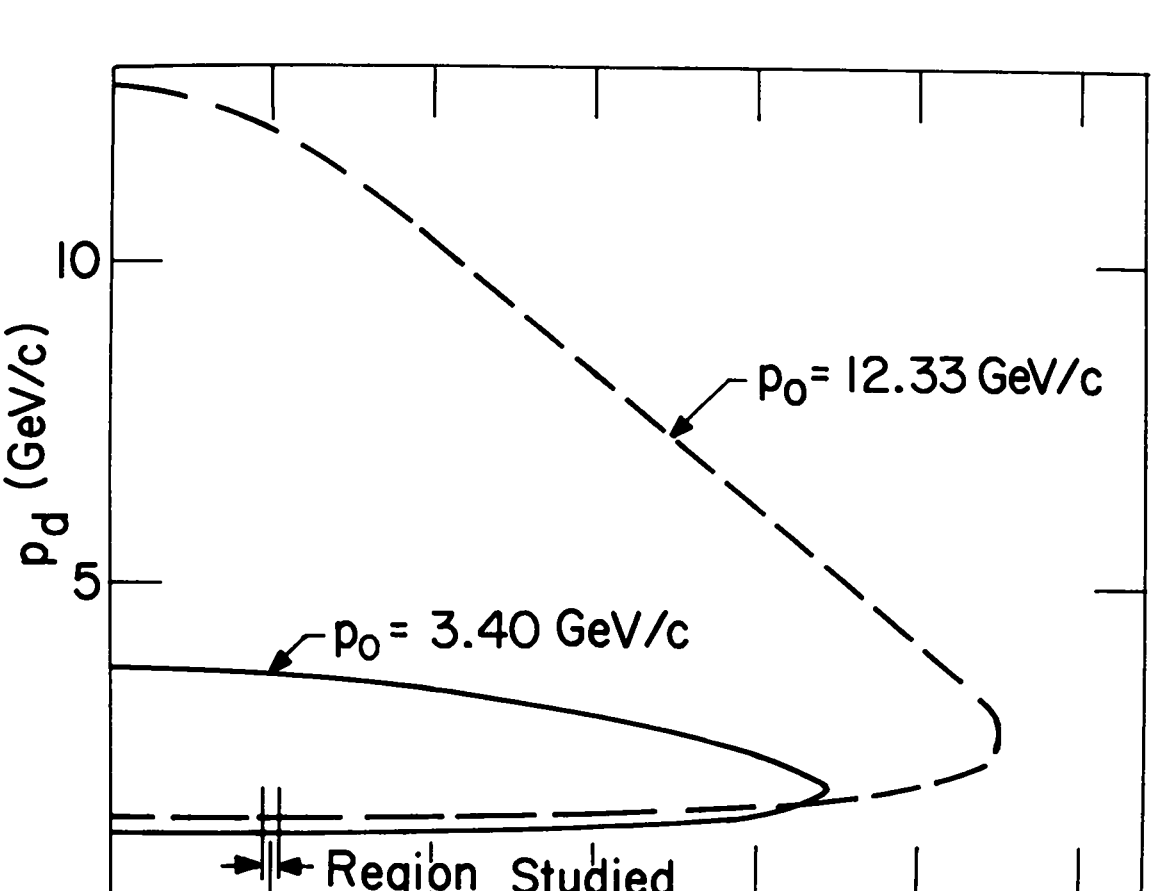
10
5
p_d (GeV/c)
p_0 = 12.33 GeV/c
p_0 = 3.40 GeV/c
Region Studied
0
5
10
15
20
25
30
θ_d (Degrees)

Fig. 2.

where θ_d is the angle between the incoming proton and outgoing deuteron, p_o and p_d are the magnitude of the incoming proton and outgoing deuteron three-momenta, and m and M are the proton and deuteron masses. Hence, by requiring particle 3 to be a deuteron and by measuring its momentum and angle of emission, the missing-mass squared is completely determined. Reaction (1) is identified by the presence of a clear peak corresponding to the pion mass in a plot of MM^2.

The deuterons, momentum analyzed within the spectrometer, could be made distinct from much more numerous protons and pions by a time-of-flight technique. Deuterons, so identified, triggered the spark chambers and vidicon system. The images of the spark chamber tracks in the vidicons were digitized and recorded on magnetic tape. From the record of the spark chamber track locations, the deuteron trajectory through the spectrometer was reconstructed and its momentum and angle of emission calculated. Reaction (1) was identified by calculating the missing-mass and requiring it to be that of the pion. Figure 2 shows the kinematical relationship between the deuteron laboratory momentum and angle for reaction (1) for the minimum and maximum incident proton momentum observed in this experiment. The region studied corresponds to deuterons emitted backward in the c.m. system. We chose to observe the backward deuterons because their smaller laboratory momentum simplified the time-of-flight measurement. In addition, the

deuteron laboratory momentum is nearly independent of angle near 5°, which in turn implies that the missing-mass is nearly angle independent.

Experimental Layout

The missing-mass spectrometer was set up in the external proton beam (EPB) of the zero gradient synchrotron (ZGS) at the Argonne National Laboratory. A diagram of the layout is shown in Figure 3. The liquid hydrogen target was located immediately outside the shielding wall of the ring building. The hydrogen flask was a 3 in. diameter cylinder with vertical axis, constructed of 3 mil H-film, and wrapped in several layers of 1/4 mil aluminized mylar superinsulation. In order to minimize the flux of non-hydrogen deuterons in the spectrometer, the flask was suspended by its filling lines in a continuous Y-shaped vacuum pipe, which extended approximately 20 ft upstream into the ring building and 24 ft downstream along both the EPB and the secondary 5° line of this experiment.

The laboratory solid angle acceptance of the spectrometer (2.08×10^{-4} sr) was defined by a 2 ft lead collimator (3-3/4 in. width x 7-49/64 in. height) located 374 in. from the hydrogen target. After passing through the collimator, the secondary beam entered the spectrometer, which was set to accept positively charged particles. The spectrometer consisted of a quadrupole pair, two bending

Fig. 3.--Experimental arrangement.

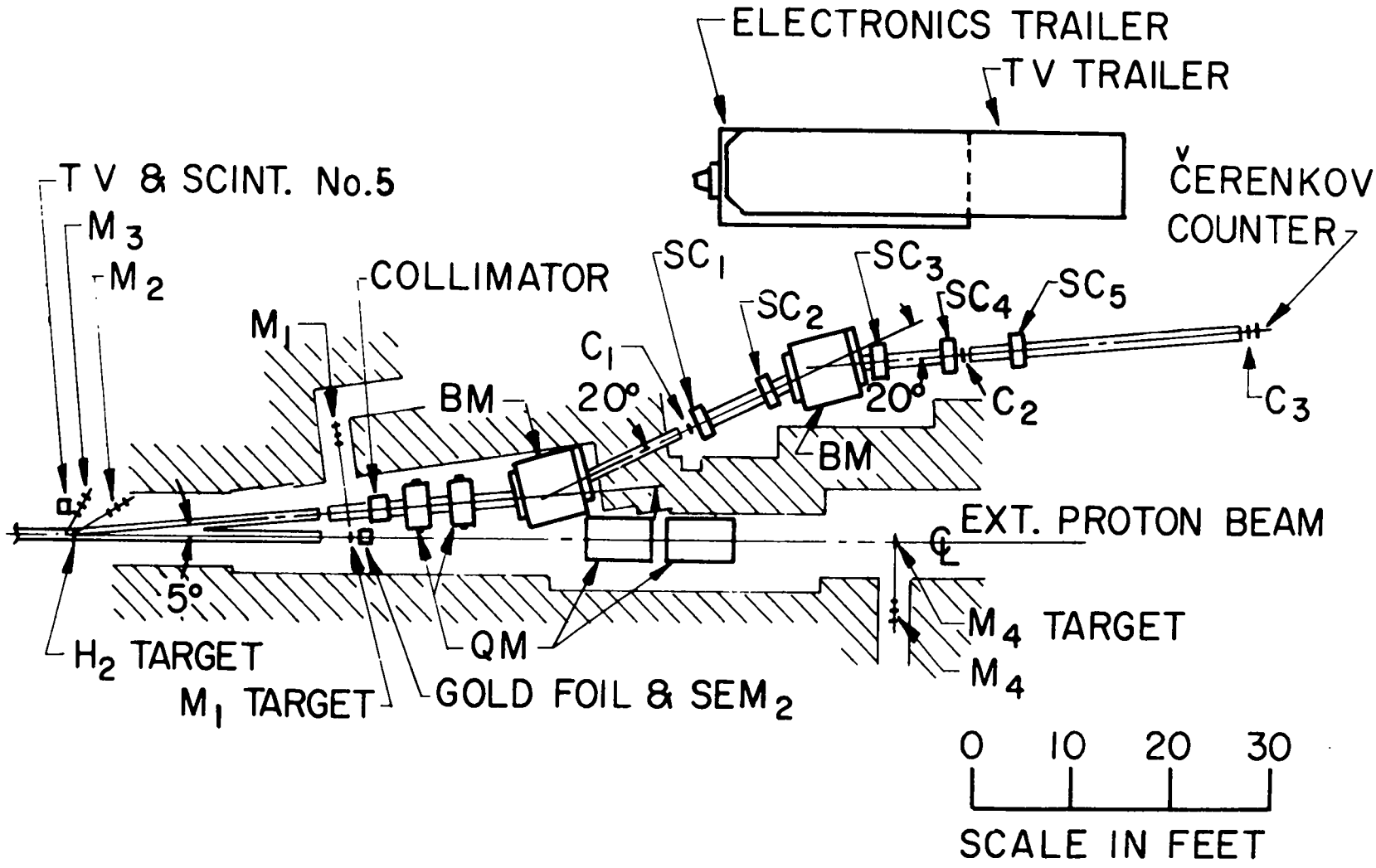
ELECTRONICS TRAILER
TV TRAILER
ČERENKOV COUNTER
T V & SCINT. No.5
M3
M2
COLLIMATOR
M1
SC1
SC2
SC3
SC4
SC5
C1
20°
BM
20°
C2
C3
BM
EXT. PROTON BEAM
5°
H2 TARGET
M1 TARGET
QM
GOLD FOIL & SEM2
M4 TARGET
M4
0 10 20 30
SCALE IN FEET

Fig. 3.

magnets in reverse bend configuration, five spark chambers with vidicon readout (SC_1, SC_2, SC_3, SC_4, and SC_5), three time-of-flight counters (C_1, C_2, and C_3), and a glycerol threshold Čerenkov counter. The distance between adjacent spark chambers on the same side of the momentum measuring magnet was 7 ft. The distance between counters C_1 and C_2 was 29 ft , as was the distance between C_2 and C_3. The first bending magnet served to bend the particles 20° in a direction away from the EPB and out of the proton tunnel. The second bending magnet served as the momentum analyzer. It was arranged to bend the particles 20° in a direction counter to the bend of the first magnet and parallel to their initial direction. All experimental apparatus after the first bending magnet was located outside of the EPB shielding wall and accessible to the experimenter at all times. A secondary emission monitor (SEM_2) and four proton beam monitors (M_1, M_2, M_3, and M_4) were located along the proton line as shown in Figure 3 and accessible only when the proton beam was off.

In order to minimize multiple Coulomb scattering of the deuterons, a helium atmosphere was maintained all along the spectrometer arm, from the end of the vacuum transport within the proton tunnel to counter C_3, with air gaps introduced only at the time-of-flight counters. The spark chambers, themselves, were maintained in a helium atmosphere. The helium transport system consisted of aluminum pipes

through the bending magnets and shielding wall with polyethylene bags connected directly to the spark chamber housings in the intervening spaces. The helium pressure was maintained at about 1/4 in. of water above atmospheric pressure by automatic pressure regulators.

The electronics trailer was centrally located with the television trailer mounted above it on a stand in order to conserve floor space in the experimental area. Figures 4 and 5 are photographs of that portion of the spectrometer arm located outside of the EPB shielding wall. Figure 4 is a view from the end of the spectrometer arm looking upstream, toward the ZGS. Figure 5 is a view taken from above time-of-flight counter C_1 looking downstream.

Proton Beam and Monitors

The EPB momentum was varied from 3.4 to 12.3 GeV/c by using a novel feature of the ZGS known as the "front porch" and illustrated in Figure 6. Also shown are signals representative of the EPB spill and the spill-gate, both of which will be discussed when gating of the electronics is taken up. The internal proton beam of about 2×10^{12} protons/pulse was accelerated up to the desired energy, a portion extracted while maintaining the ZGS field constant, and the remainder accelerated to full energy for other use. Spills were from 300 to 500 msec in length with a repetition period that varied from 2.6 to 3.5 sec. The extracted beam intensity was usually limited to about 10^{11} protons/pulse

Fig. 4.--Spectrometer looking upstream, toward the ZGS.

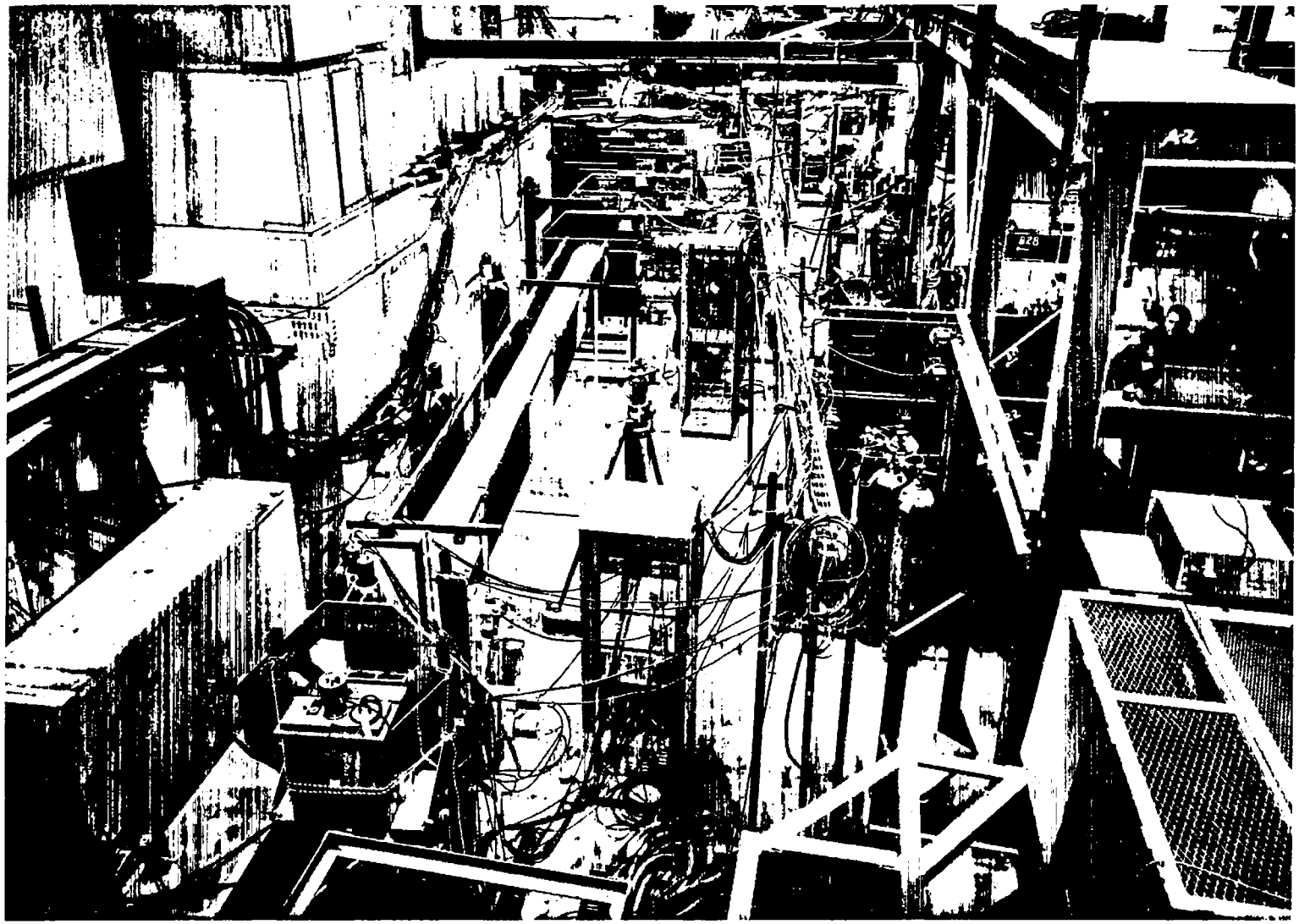

Fig. 4.

Fig. 5.--Spectrometer looking downstream, away from the ZGS.

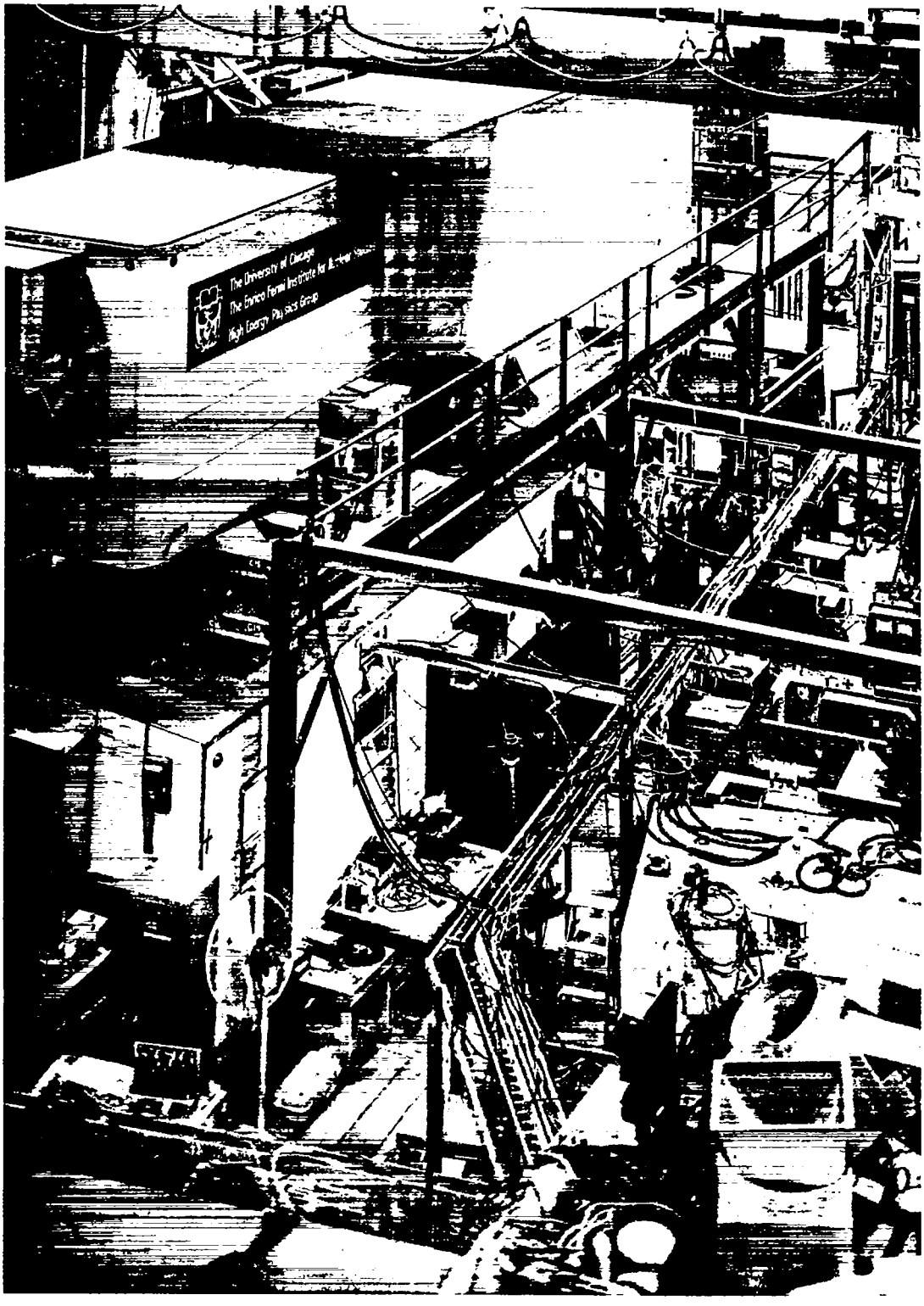
The University of Chicago
The Enrico Fermi Institute for
High Energy Physics Group

Fig. 5.

Fig. 6.--A partial ZGS magnetic field cycle showing the proton beam extracted during the "front porch." Also shown is the gating level which permits the electronics to count during extraction.

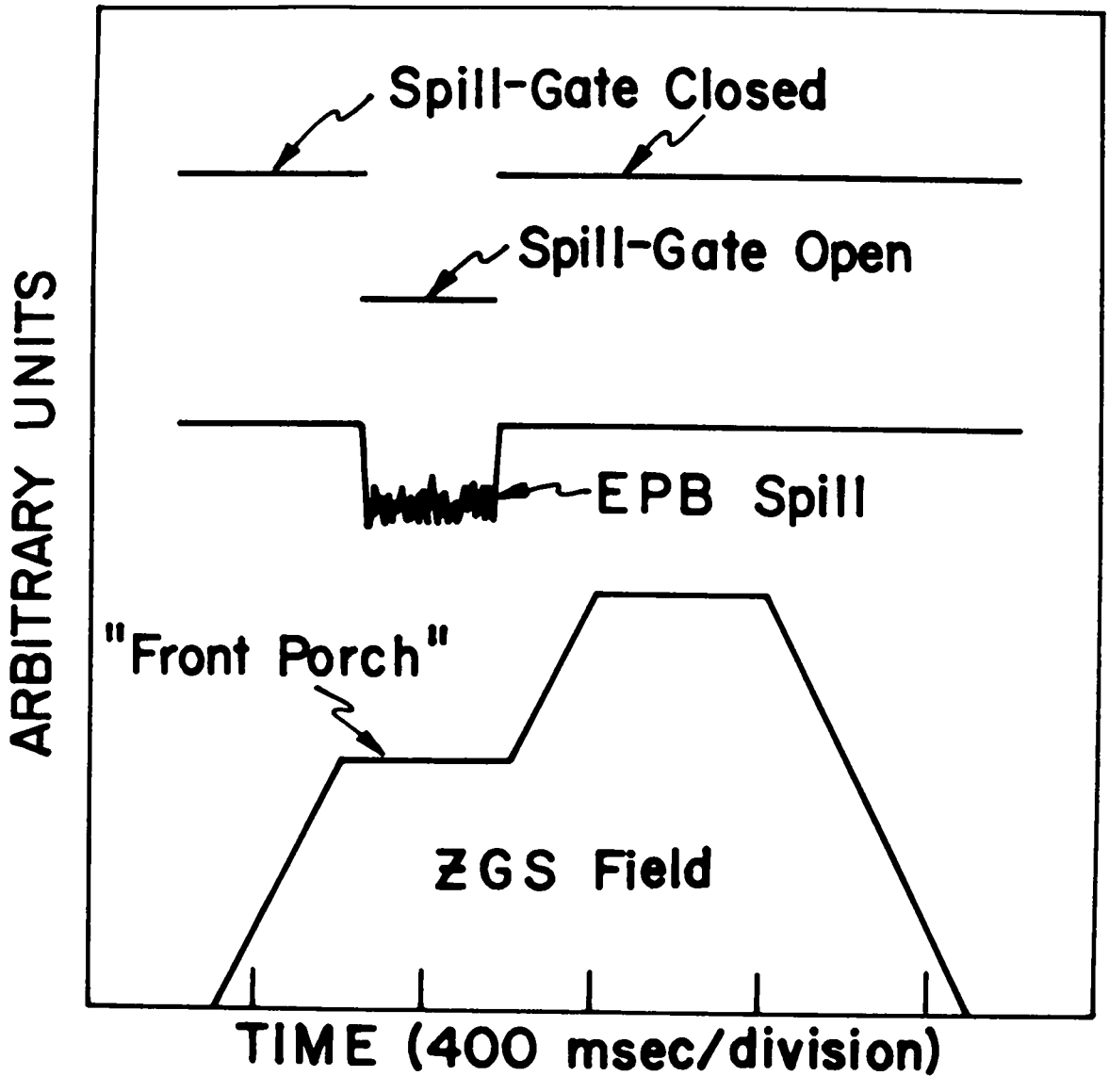
Spill-Gate Closed
Spill-Gate Open
EPB Spill
"Front Porch"
ZGS Field
ARBITRARY UNITS
TIME (400 msec/division)

Fig. 6.

so as not to exceed about 1.5×10^5 particles/pulse in the first spark chamber SC_1. The beam had a momentum spread of about $\pm$ 10 MeV/c and an absolute energy calibration correct to about $\pm$ 1/2%.

The determination of the differential cross section for reaction (1) required a knowledge of the absolute number of protons that traversed the hydrogen target during a particular measurement. However, the proton beam intensity could not be measured directly by conventional counting techniques due to the high EPB rate (10^{11} to 10^{12} protons/sec). Therefore, the protons were counted indirectly by monitor M_1 which observed the secondary spray from the EPB when it struck a 1/4 in. thick Plexiglas target located on a flip-stand 25 ft downstream of the hydrogen target and immediately upstream of the SEM_2 stand (see Figure 3). Monitor M_1 (as well as M_2, M_3, and M_4) consisted of a linear array of three identical counters in coincidence. The counters were constructed of easily changed NE102 plastic scintillators, air light guides, and either RCA 8575 or Amperex 56 AVP photomultipliers. The size of the scintillators used depended upon the rates at the monitor and was typically 1/2 sq. in. in area by 1/4 in. thick. The monitor M_1 counts were in turn related to the absolute number of protons in the EPB by gold foil activation which consisted of counting the α -branch of Tb^{149} produced in gold by proton bombardment. The techniques used were established

for the EPB of the ZGS and are discussed in detail by Steinberg et al.[14] We shall return to this subject later.

A diagram of the EPB transport system from the ZGS ring to the hydrogen target, as it existed at the time of this experiment, is shown in Figure 7. The proton line was tuned using a diagnostic system of television cameras and monitor telescopes. The beam could be observed, via television, striking grided Pilot B plastic scintillators located along the transport system as indicated in Figure 7. These scintillators could be flipped out of the beam when not in use. As shown in Figure 3, monitor M_2 viewed the hydrogen target. It aided in centering the beam on the target as well as giving a continuous check on the status of the target. Monitor M_3 viewed a section of the vacuum pipe immediately upstream of the hydrogen target. Deviations of M_3 from its nominal value were a good indication that the beam was wiping off on the transport system upstream. The secondary emission monitor (SEM_2) was used for checking the instantaneous beam intensity as well as the transport efficiency from the ZGS ring by comparing it with SEM_1, located just outside the ring (see Figure 7). Monitor M_4 viewed a Plexiglas target (6 in. x 6 in. x 5/32 in.) mounted on a motorized table top and

---

[14] E. P. Steinberg, A. F. Stehney, Carole Stearns, and Irene Spaletto, Nucl. Phys. A113, 265 (1968).

Fig. 7.--External proton beam transport system from the ZGS ring to the hydrogen target immediately outside the shielding wall of the ring building.

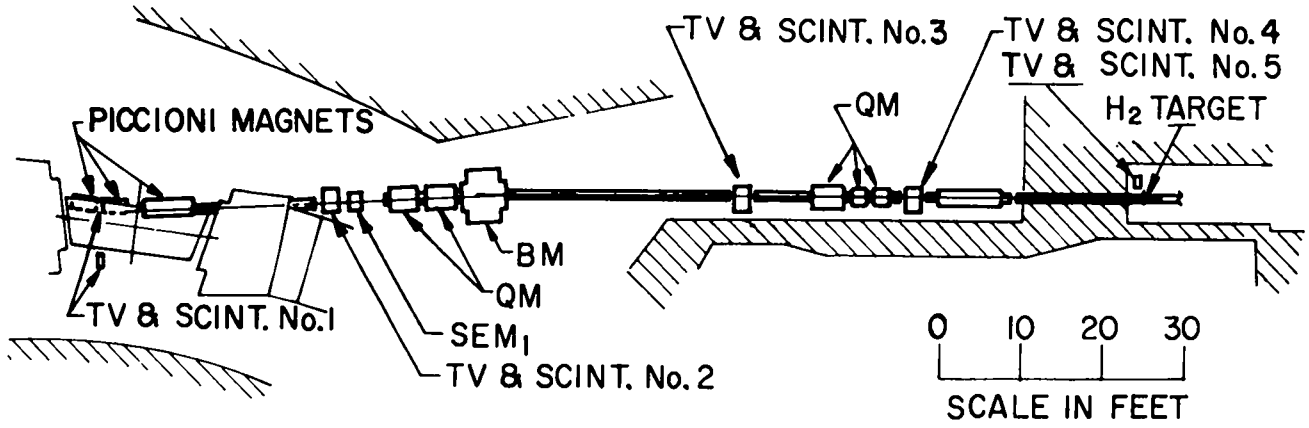
TV & SCINT. No.3
TV & SCINT. No.4
TV & SCINT. No.5
QM
H2 TARGET
PICCIONI MAGNETS
BM
QM
TV & SCINT. No.1
SEM1
TV & SCINT. No.2
0 10 20 30
SCALE IN FEET

Fig. 7.

located approximately 80 ft downstream of the hydrogen target. It was used for checking the beam centering for other users downstream.

As can be seen from Figure 7, the EPB transport system, upstream of this experiment, consisted of three Piccioni extraction magnets, a quadrupole pair, a bending magnet, and a quadrupole triplet. A quadrupole pair was located downstream of the SEM_2 stand, as shown in Figure 3, in order to refocus the beam for other users. Preliminary EPB transport solutions were obtained by computer and the final operating conditions by empirical tuning. Acceptable conditions were reached by centering the beam on the TV scintillators, maximizing M_2 while minimizing M_3, centering the beam with M_4, and checking the spectrometer rates with an empty target. A Polaroid film was exposed at the M_1 target to check beam position and angular divergence. The cross section and angular divergence of the EPB at the hydrogen target often represented a compromise between the desired conditions and the requirements downstream of other users. The cross section was usually less than about 3 cm^2 and the angular divergence did not exceed ± 5 mrad in either the horizontal or vertical plane. The beam was close to a focus at the hydrogen target.

Spectrometer

The length of the flight path for the time-of-flight measurement, the momentum resolution, and the width of the momentum acceptance were the factors of prime concern in the choice and placement of the magnetic elements of the spectrometer. The momentum measuring error and the uncertainty in momentum due to the energy loss of the deuterons in the target are the principal contributors to the uncertainty in the calculation of the missing-mass. For a given target size, therefore, it was only necessary to seek a momentum resolution of the order of the energy loss of the deuterons in the target.

Since the backward deuterons from reaction (1) are nearly monoenergetic, a large momentum bite was not required for its study. However, in order to study bosons of mass greater than the pion, it was desirable to design the spectrometer with as large an acceptance as possible. On the other hand, the particle flux that spark chamber SC_1 could tolerate and the difficulty of separating deuterons from protons and pions at high spectrometer momenta were two reasons for limiting the momentum bite.

The spectrometer was designed with the aid of a computer program which calculated the transport matrix elements at each piece of restricting apparatus placed in the beam (collimator, magnets, counters, and spark chambers).

The transport equations in the horizontal direction from the target to the point of interest are given by the matrix equation

$$\begin{pmatrix} x \\ dx/dz \\ (p_d-p_s)/p_s \end{pmatrix} = \begin{pmatrix} C(z) & S(z) & D(z) \\ C'(z) & S'(z) & D'(z) \\ 0 & 0 & 1 \end{pmatrix} \begin{pmatrix} x_o \\ (dx/dz)_o \\ (p_d-p_s)/p_s \end{pmatrix}$$

where p_d is the deuteron laboratory momentum, p_s is the central spectrometer setting, x is the perpendicular displacement from the optical axis in the horizontal plane, and z is the distance along the optical axis. The elements of the transport matrix are a function of the distance along the optical axis and the types of magnetic fields traversed.[15]

The magnetic elements of the spectrometer consisted of a quadrupole pair and two bending magnets in reverse bend configuration. The quadrupoles (ZGS designation QM-104) had a 10-1/8 in. bore, 19.4 in. effective length, and a minimum focal length of 30 in. at 1 GeV/c. The first bending magnet (ZGS designation BM-105), located just inside the EPB shielding, had a 15.2 in. horizontal by 6 in. vertical gap and a maximum $\int B \cdot dl$ of 3400 kG cm. The momentum measuring magnet (ZGS designation BM-109) had a 24 in.

---

[15] S. Penner, Rev. Sci. Instr. 32, 150 (1961).

horizontal by 8 in. vertical gap and a maximum $\int B \cdot dl$ of 3500 kG cm. The effective length of the bending magnets was measured using two search coils on opposite ends of an adjustable rod. The plane of the coils was aligned perpendicular to the magnetic field. The coils were moved along the length of the magnet in such a manner that one coil was entering the magnetic field as the other was departing it. The motion of the coils was stopped when the centerline of the connecting rod was aligned with the centerline of the magnet and the net change in flux between the coils noted. The effective length was determined by that distance between the coils for when no net change in flux was observed. A series of effective length measurements were made while varying the magnetic field and a third order relation between the two established. The effective length, as determined by this technique, was accurate to better than $\pm 0.1\%$.

The distance between spark chambers, which influences the momentum resolution, and the distance between bending magnets, which influences the momentum acceptance, were both limited by the over-all space requirements. Therefore, the momentum resolution and the momentum acceptance were determined primarily by the angle of bend of the spectrometer. Increasing the bending angle increased the resolution and decreased the acceptance. Increasing the flight path also decreased the momentum acceptance.

The 5^{o} emission angle of the deuterons was chosen in order to be as close as possible to 0^{o} without going into the EPB with a magnet. The first bending magnet in the spectrometer was necessary because of the small production angle being observed and the need to get the secondary beam away from the EPB and out of the proton tunnel. The spectrometer bending angle was chosen at 20^{o}. This provided sufficient working space for the spectrometer, an adequate momentum measuring resolution of $\pm$ 1/3%, and an acceptable momentum bite of $\pm$ 4%.

The magnets were arranged in the reverse bend configuration in order to compensate for the angular dispersion introduced by the first bending magnet. This could be arranged to give a zero value for the matrix element $D'(z)$ and a constant value for the matrix element $D(z)$ after the second bending magnet. Such a setting permitted the use of existing 10 in. x 10 in. spark chambers and a long flight path after the second bending magnet without seriously limiting the momentum acceptance. The quadrupoles helped provide a relatively large solid angle. By choosing the horizontal focus near counter C_3, the displacement from the optical axis after the second bending magnet did not depend strongly on the initial deuteron angle. At C_3 ($S(z) \approx 0$) the displacement was independent of the initial deuteron angle and depended primarily on the deuteron momentum, at least for a point source ($x_o = 0$). Therefore, the

spatial dispersion at C_3 was determined by the matrix element D(z) which was 3 mm per MeV/c at 1 GeV/c. The vertical focus was chosen near the center of the second bending magnet in order to maximize the solid angle.

Figure 8 shows the spectrometer acceptance, $(p_d-p_s)/p_s$ versus laboratory angle θ_d, for central spectrometer momentum p_s = 1.14 GeV/c as calculated with the aid of the computer program for the experimental arrangement shown in Figure 3. Included in the acceptance window is the kinematic line for reaction (1) for p_o = 3.4 GeV/c. Also indicated in Figure 8 are the aperatures which limit the acceptance. The target was treated as a point source. The angular acceptance of $\pm$ 0.3° ($\pm$ 5 mrad) at the central momentum was fixed by the collimator. Without the collimator the angular acceptance at the central momentum would have been limited by the second quadrupole at $\pm$ 8.5 mrad. If counter C_3 had been the only aperture limiting the momentum bite, the acceptance would have been rectangular in good conformity with the pion-mass line, which is almost horizontal in the region investigated. However, as can be seen in Figure 8 spark chambers SC_3 to SC_5 did cut into the acceptance somewhat, thus limiting the momentum bite to about $\pm$ 2.7% while still accepting the full angular spread of the central momentum of $\pm$ 5 mrad.

The actual acceptance of the spectrometer does not have the sharp outline indicated in Figure 8 but has fuzzy

Fig. 8.--Acceptance window for the spectrometer as calculated by the matrix technique for incident proton momentum p_o = 3.4 GeV/c and spectrometer setting p_s = 1.14 GeV/c. Shown in the window is the kinematic line for the pion missing-mass, MM = 0.140 GeV. The momentum bite is limited by time-of-flight counter C_3 and spark chambers SC_3 and SC_5. The angular acceptance is limited by the collimator.

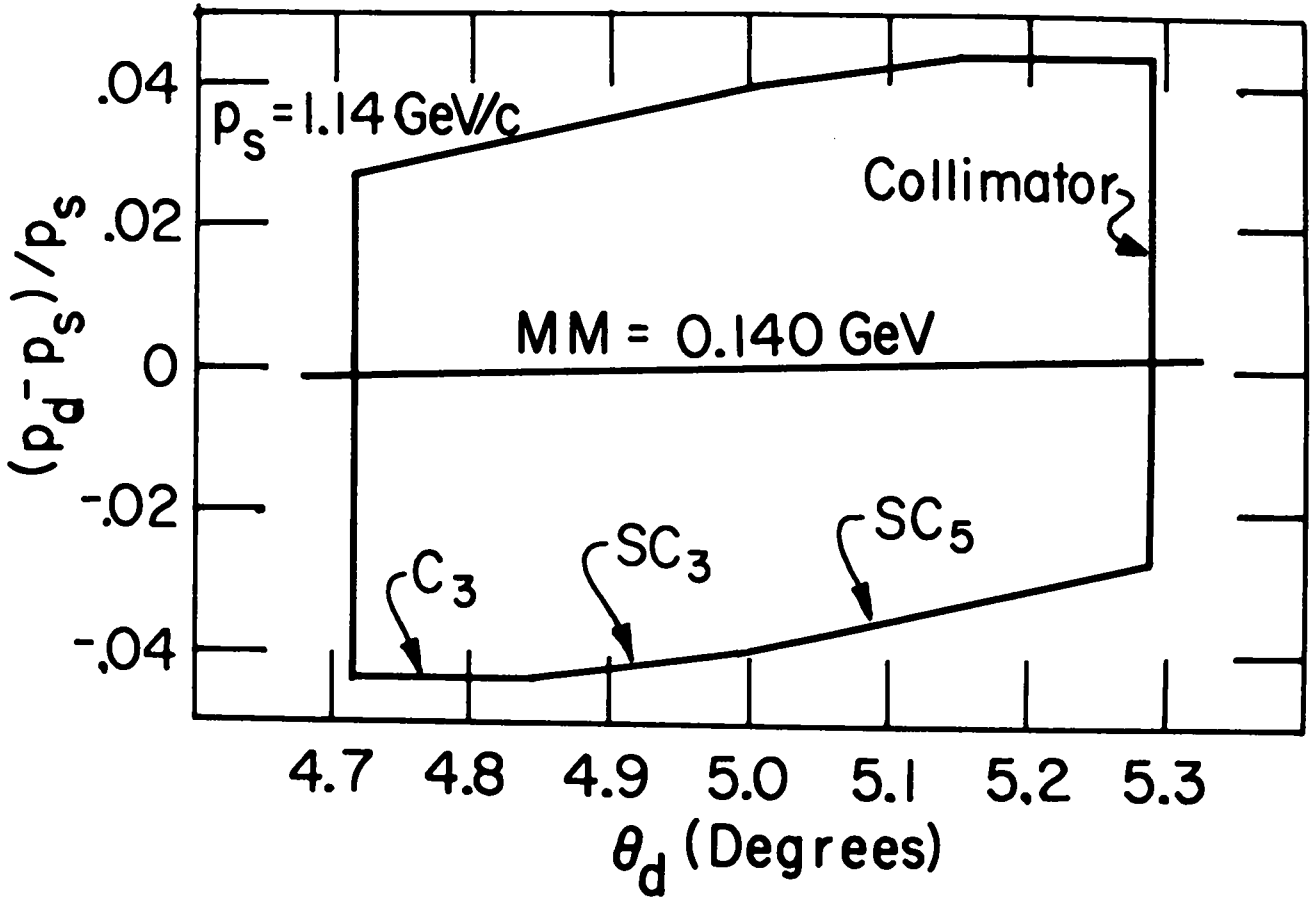
.04
.02
0
-.02
-.04
$(p_d - p_s)/p_s$
p_s = 1.14 GeV/c
Collimator
MM = 0.140 GeV
C_3
SC_3
SC_5
4.7
4.8
4.9
5.0
5.1
5.2
5.3
θ_d (Degrees)

Fig. 8.

Fig. 9.--Spectrometer efficiency as calculated by a Monte-Carlo program which randomly chose the events and traced them through the spectrometer for $p_s = 1.14$ and 1.34 GeV/c. The fact that the efficiency curves do not reach 100% at the central spectrometer setting is a measure of the losses from multiple Coulomb scattering. The points are an experimental measurement of the spectrometer efficiency using deuterons from the reaction $p + p \rightarrow d + \pi^+$ with momentum $p_d = 1.18$ GeV/c. The spectrometer window was swept across the pion mass line and the deuteron yield measured as a function of spectrometer setting p_s. The experimental points are normalized to the yield at the central value $p_s = 1.18$ GeV/c and adjusted to reflect the loss from multiple scattering. The size of the experimental points indicate the statistical error.

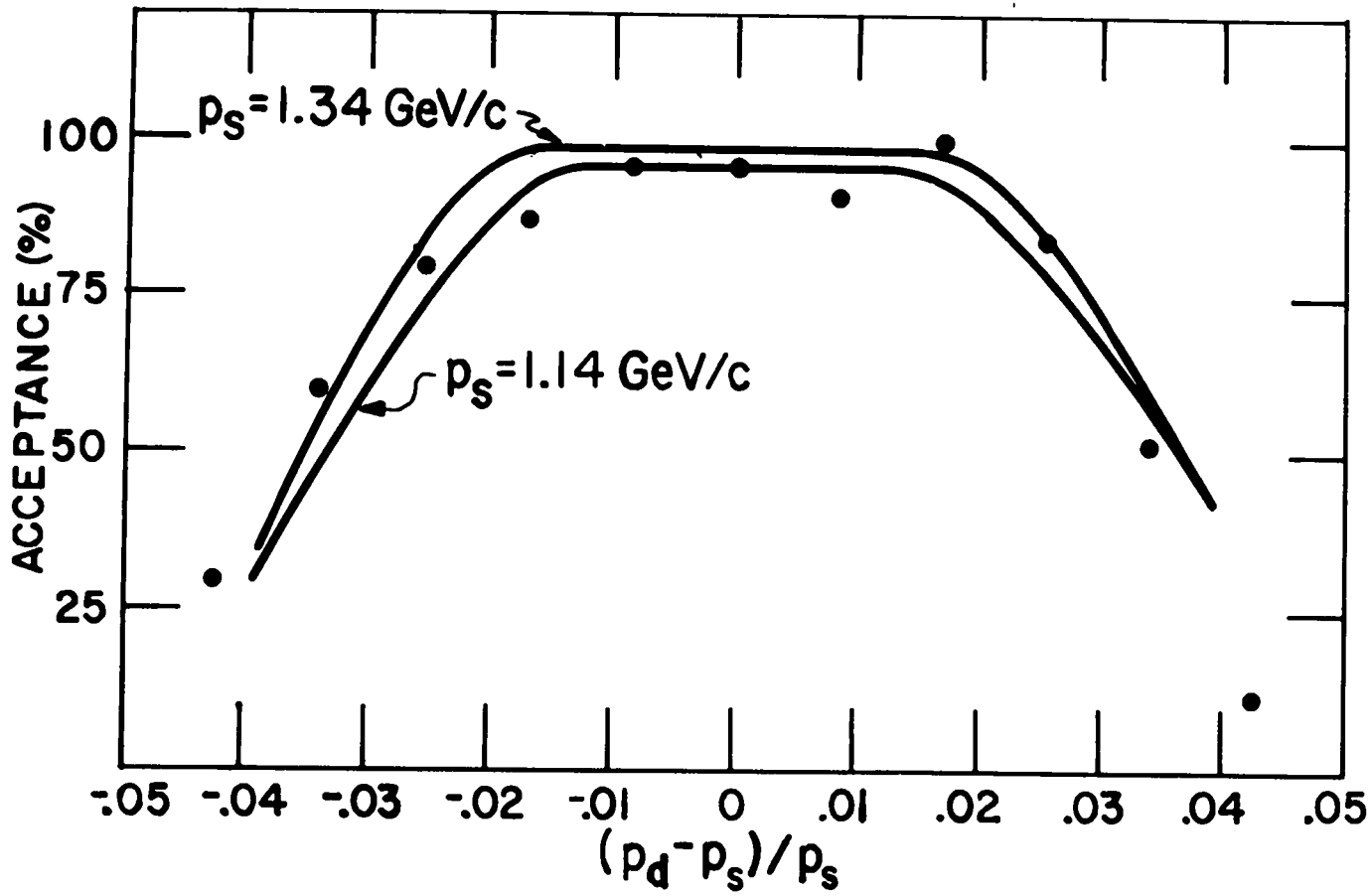
p_s=1.34 GeV/c
p_s=1.14 GeV/c
ACCEPTANCE (%)
100
75
50
25
-.05
-.04
-.03
-.02
-.01
0
.01
.02
.03
.04
.05
$(p_d - p_s)/p_s$

Fig. 9.

edges because of the finite target size and the multiple Coulomb scattering of the deuterons. Therefore, a Monte-Carlo program was written to compute this acceptance. The Monte-Carlo program randomly chose the three coordinates of the vertex in the target, the deuteron momentum, and the angle of emission of the deuteron. It traced the deuteron through the spectrometer, taking into account energy loss and multiple scattering.[16] Figure 9 shows the spectrometer efficiency curves for deuterons which pass through the collimator and ultimately reach counter C_3 versus $(p_d-p_s)/p_s$ for spectrometer momenta of 1.14 and 1.34 GeV/c, as computed by the Monte-Carlo program. Also shown in Figure 9 are the points corresponding to an experimental measurement of the spectrometer efficiency, discussed below. The Monte-Carlo calculation shows that the acceptance is flat for about $\pm$ 1.5% of the central momentum. All deuterons that passed through the collimator within this momentum range were accepted by the spectrometer, except for a small loss from multiple scattering. From the results of the Monte-Carlo calculation, the scattering loss at 1.14 GeV/c and 1.34 GeV/c was found to be 4.7% and 1.3%, respectively. The program was run at several other intermediate momenta in order to correct the differential cross sections of reaction (1) for loss by multiple scattering.

---

[16] W. H. Barkas and A. H. Rosenfeld, UCRL-8030 Rev. (1961).

At an incident proton momentum of 4.0 GeV/c, the spectrometer acceptance was measured using deuterons from reaction (1). This was accomplished by moving the spectrometer window across the pion mass line and observing the drop in yield from reaction (1) as the mass line moved out of the window. At p_o = 4.0 GeV/c the deuterons from reaction (1) have a momentum of 1.18 GeV/c. Therefore, the spectrometer was swept across the pion mass line from 1.13 to 1.24 GeV/c in steps of 0.01 GeV/c. The resulting measurements, normalized to the yield at p_s = 1.18 GeV/c and adjusted to include the multiple Coulomb scattering loss, are plotted in Figure 9, and they are in good agreement with the acceptance calculated by the Monte-Carlo program.

Counters and Electronics

Identification of reaction (1) required first separating deuterons, whether originating from the hydrogen target or not, from an intense background of protons and pions. Within the spectrometer, the protons and pions had fluxes several hundred times greater than that of the deuterons. The deuterons were identified by selecting particles with momenta in a specified range (approximately $\pm$ 4% of the central spectrometer momentum) and then measuring the time-of-flight of those particles. For the momenta of interest in this experiment (p_d = 1.14 to 1.34 GeV/c),

deuterons had a $\beta \approx 0.5$ ($\beta = 1$ being the speed of light), protons a $\beta \approx 0.75$, and pions a $\beta \approx 1$. Therefore, deuterons could be easily separated from the less massive protons and pions with a reasonable flight path. Although the spectrometer was not operated above 1.34 GeV/c in order to study reaction (1), it was designed to operate as high as 3 GeV/c in order to study more massive bosons. At 3 GeV/c, the deuteron-proton separation is less than 4 nsec over a flight path of 29 ft. Therefore, it becomes difficult to separate deuterons from protons and pions in this region and considerable attention was devoted to maximizing the resolution of the time-of-flight system.

It should also be noted at this point that, since the backward deuterons from reaction (1) in the vicinity of 5° in the laboratory are nearly monoenergetic for a fixed incident proton energy, the time-of-flight measurement not only affords an opportunity of separating deuterons from all other particles, it also presents the possibility of identifying the deuterons from reaction (1). This is true, of course, provided the signal-to-background ratio for reaction (1) is favorable. Identification of reaction (1) by time-of-flight alone provided further motivation for maximizing the resolution of the time-of-flight system. With the spectrometer set on the deuteron momentum for reaction (1), the time-of-flight distribution for deuterons should appear with a sharp peak centered on a broad background of

non-hydrogen deuterons. The differential cross section for reaction (1) can then be extracted from the time-of-flight data without reference to the spark chambers. This technique was employed during data taking, and it provided an important experimental check, as will be discussed below.

Some of the factors limiting the resolution of a time-of-flight measurement include: the variation in length of the flight path for off-axis trajectories through the spectrometer, the position variation of the particles in the scintillators, the decay time of the scintillator, the transit time spread of the electrons through the photomultipliers, the degradation of the rise time of the photomultiplier tube pulses in long transmission cables, and the type of discriminators and coincidence circuits employed. In counters employing large scintillators, the position variation of the event within the scintillator and the subsequent transit time spread of the photons to the photomultiplier can contribute significantly to the timing uncertainty of the event. For the size of the counters used in this experiment, the vertical position spread could have introduced an uncertainty of about $\pm$ 1.5 nsec. This uncertainty can be cut in half by viewing the scintillator at the upper and lower edges and merely accepting the first photomultiplier to fire. We have, however, made use of the fact that the sum of the transit time of the direct light from the event to opposite edges of the scintillator is a

Fig. 10.--Scintillator and photomultiplier tube arrangement for time-of-flight counters C_1 and C_2. The scintillator was viewed at opposite edges for improved time resolution.

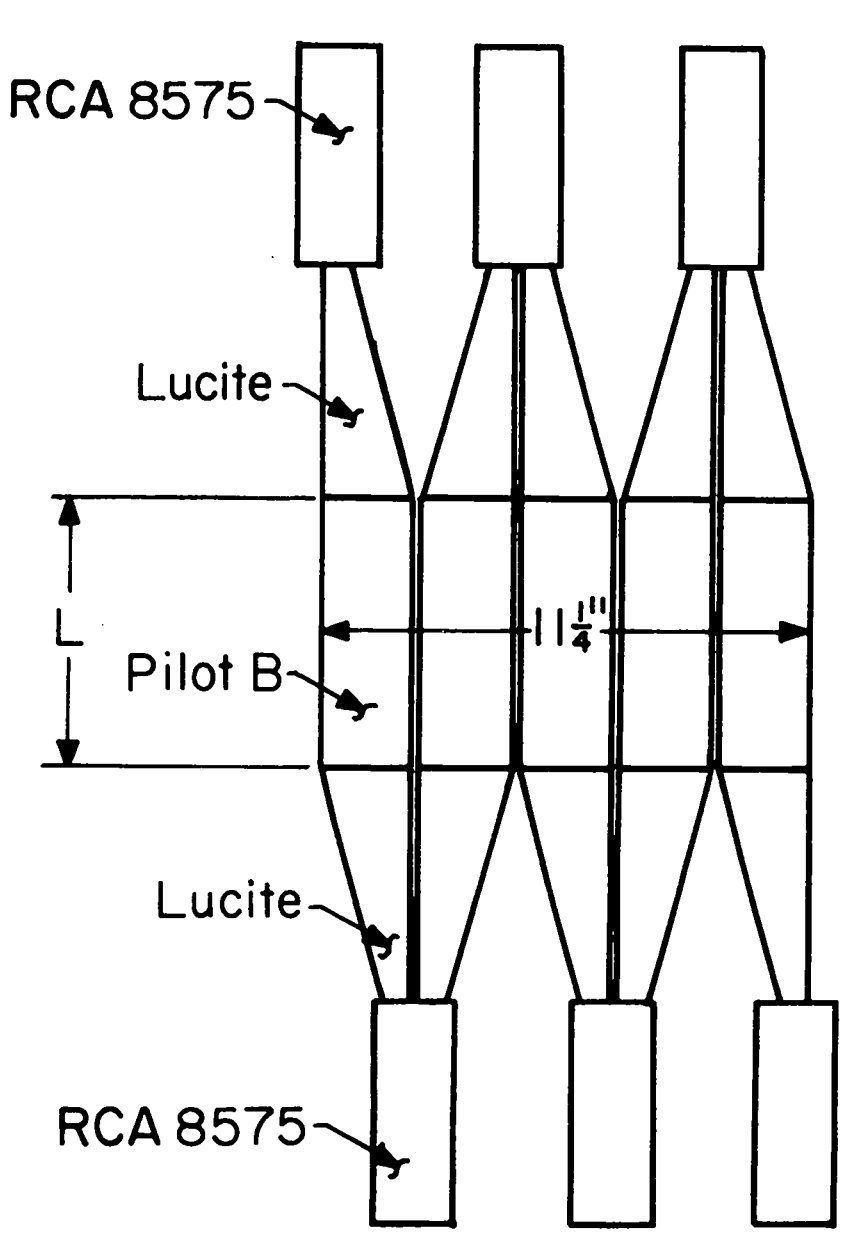
RCA 8575
Lucite
L
Pilot B
11 1/4"
Lucite
RCA 8575
L = 7" for C1
L = 11" for C2

Fig. 10.

constant and independent of position. If the time-of-flight between the same pair of counters is measured twice, employing the upper tubes for one measurement and the lower tubes for the other measurement, and if the two measurements are added, the vertical position spread can be essentially cancelled.

Time-of-flight counters C_1 and C_2 each consisted of five 1/8 in. thick by 2-1/4 in. wide Pilot B plastic scintillators viewed at both the upper and lower end by RCA 8575 photomultipliers. These are 12 stage tubes with a 2 to 3 nsec rise time and were operated at about 2000 V. Each counter required six tubes. The photomultipliers and scintillators were optically cemented with NE580 to tapered Lucite light guides. The scintillators and light guides were optically separated from each other by 1/2 mil aluminum foil and arranged as shown in Figure 10, thus giving hodoscope capabilities in the horizontal direction to the counters, as well as improved time resolution. Counters C_1 and C_2, along with their associated local logics, were identical except for the length of the scintillators, which was 7 in. and 11 in., respectively. Counter C_3 consisted of a single sheet of NE102 plastic scintillator (11 in. x 11 in. x 1/4 in.) which was viewed at both the upper and lower end by an RCA 8575 photomultiplier. The photomultipliers and scintillator were cemented with NE580 to commercial, twisted Lucite light guides.

In order to minimize the cable length through which the raw photomultiplier tube pulses were required to travel, a system of local logics was placed within close proximity (5-10 ft) to each of the time-of-flight counters. All photomultiplier tube pulses to zero-crossing discriminators at the local logics were carried by 50 Ω , RG223 cable. Logic pulses from the local logics to the electronics trailer were carried by 50 Ω air core cable, HJ-50 manufactured by Andrew Corporation, over an average distance of about 50 ft in an effort to reduce time delay and signal attentuation. The electronic circuitry at both the local logics and in the electronics trailer largely used M100 modules manufactured by Edgerton, Germeshausen and Grier, Inc. Figure 11 gives a block diagram of the local logics for either C_1 or C_2. It is apparent that five two-fold coincidences were required per counter in order to define the scintillator through which the particle passed. These hodoscope coincidences were formed, apart from the time-of-flight circuitry, at the local logics, eventually strobed by a deuteron event, and recorded on magnetic tape to be used in the analysis for cross checking the spark chamber retrace. As indicated in Figure 11, all upper tubes were ORed together, and all lower tubes were ORed together. The input pulses at the OR circuits were timed to within about 1/10 nsec using General Radio constant impedance trombones and time-to-amplitude converters (TAC), discussed later. The 2 of 6

Fig. 11.--Block diagram of the electronic circuitry for either time-of-flight counter C_1 or C_2. This system of local logics was placed in close proximity (5 to 10 ft.) to each counter.

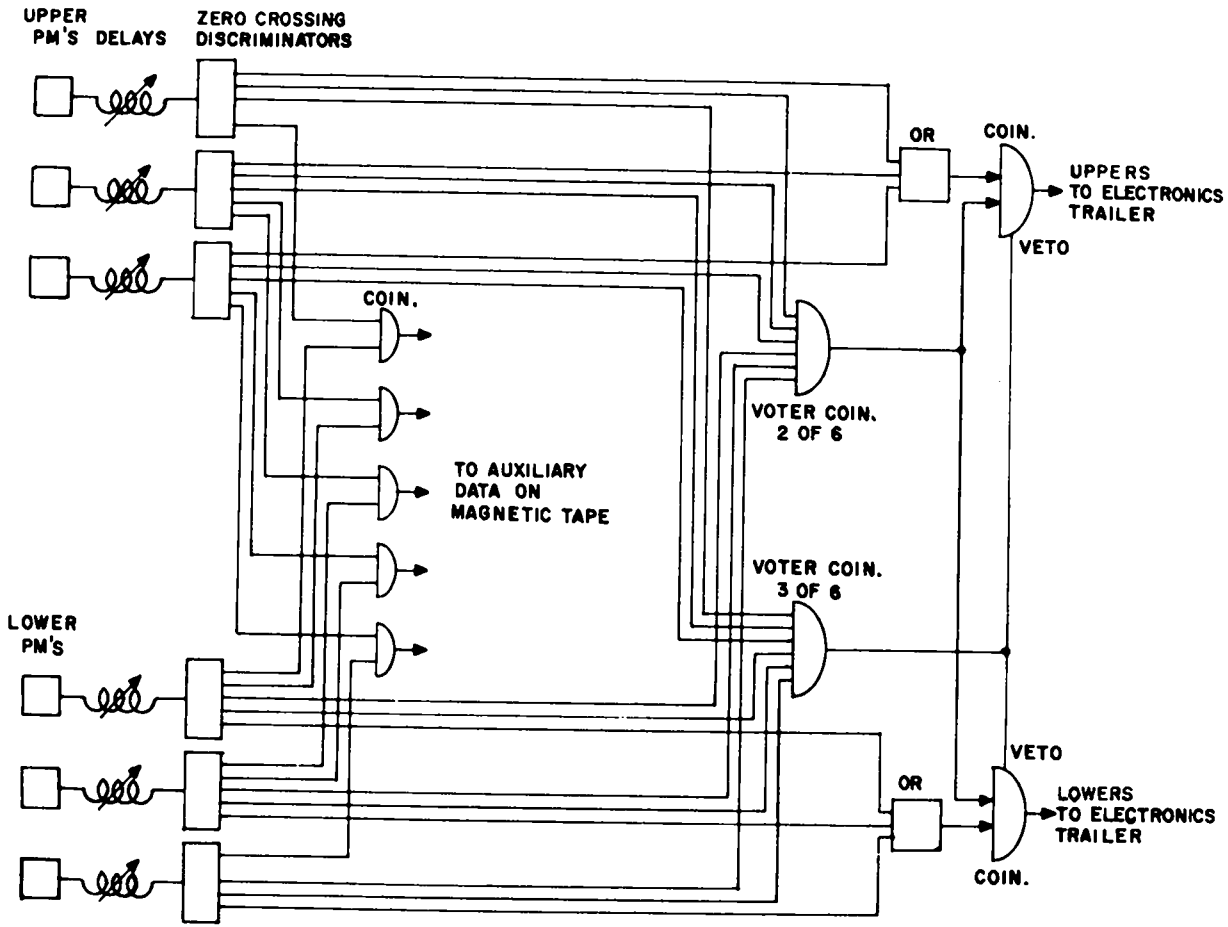
UPPER PM'S
DELAYS
ZERO CROSSING DISCRIMINATORS
OR
COIN.
UPPERS TO ELECTRONICS TRAILER
VETO
COIN.
TO AUXILIARY DATA ON MAGNETIC TAPE
VOTER COIN. 2 OF 6
VOTER COIN. 3 OF 6
LOWER PM'S
VETO
OR
LOWERS TO ELECTRONICS TRAILER
COIN.

Fig. 11.

Fig. 12.--Block diagram of the main logics in the electronics trailer.

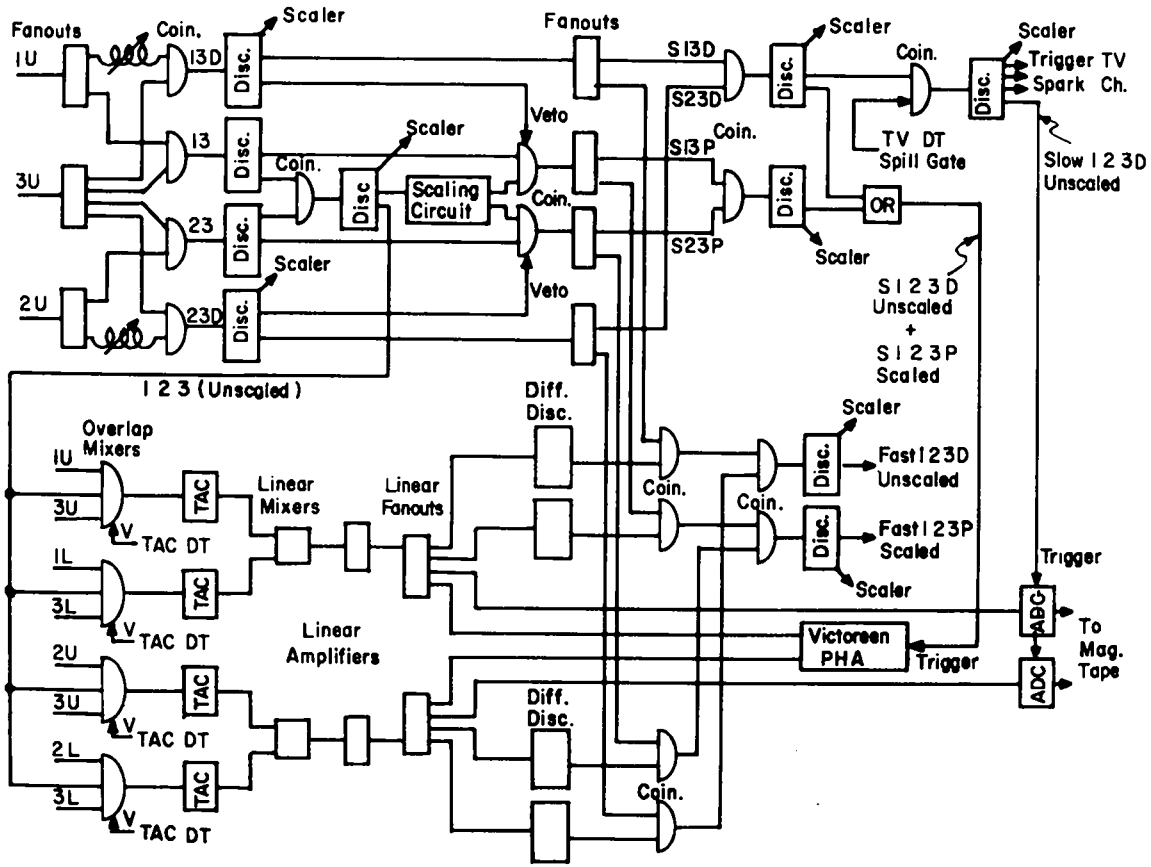
Fanouts
1U
Coin.
13D
Disc.
Scaler
13
3U
23
2U
23D
Scaling Circuit
Veto
1 2 3 (Unscaled)
Fanouts
S13D
S23D
S13P
S23P
Coin.
Scaler
TV DT Spill Gate
OR
Trigger TV
Spark Ch.
Slow 1 2 3D Unscaled
S 1 2 3D Unscaled + S 1 2 3P Scaled
Overlap Mixers
1U
3U
1L
3L
2U
3U
2L
3L
TAC
TAC DT
Linear Mixers
Linear Fanouts
Linear Amplifiers
Diff. Disc.
Fast 1 2 3D Unscaled
Fast 1 2 3P Scaled
Victoreen PHA
Trigger
ADC
To Mag. Tape

Fig. 12.

voter coincidence requirement assured that a particle had passed through the counter, thus blocking photomultiplier tube noise. The 3 of 6 veto cancelled any event where two particles passed through two different scintillators of the same counter within about 20 nsec of each other. This helped to reduce accidental coincidences where an initial particle could trigger only C_1 and a later particle, less massive than the deuteron, could traverse the complete time-of-flight telescope and fake a deuteron. The local logics for C_3 consisted of merely gating the upper tube and the lower tube, separately, by the same upper-lower coincidence before transmitting them to the electronics trailer.

Figure 12 is a block diagram of the main logics in the electronics trailer. The time-of-flight was measured twice, over the complete flight path of 58 ft by a C_1C_3 coincidence and over the last 29 ft of the flight path by a C_2C_3 coincidence. An event required a coincidence between the two time-of-flight measurements. Therefore, counters C_1 and C_3 and counters C_2 and C_3 were combined in parallel circuits in both the slow section, using conventional coincidence techniques, and the fast section, using time-to-amplitude converters. The slow 13D and 23D were formed by varying the delay of 1 and 2, as well as the width of 1 and 2, relative to 3 as the momentum of the spectrometer was changed. In this way deuterons could be kept in time,

while excluding other particles, as the deuteron-proton time-of-flight difference varied. In the slow section raw 123 coincidences were scaled down by powers of 10 (usually 1000) and brought back into coincidence with both the 13 and the 23, which were set to accept everything, pions, kaons, protons, and deuterons. Eventually, there was formed an unscaled slow 123 timed for deuterons (S123D) and a scaled slow 123 which included everything minus deuterons (S123P). The slow section required only the upper tubes of the time-of-flight counters.

The electronic circuitry of the fast section was designed to minimize the effects of the vertical position spread in the counters in the manner suggested, that is, measuring the time-of-flight between the same pairs of counters twice and adding the resulting measurements. Consequently, the upper tubes were used to trigger one coincidence circuit (overlap mixer) and its accompanying TAC while the lower tubes triggered a parallel circuit. The output of the upper and lower TAC's was added in a linear mixer. The output of the linear mixer, after amplification, was sent to an amplitude-to-digital converter which was triggered by the event. The time-of-flight for each event was subsequently recorded on magnetic tape. This procedure was followed for both the C_1C_3 and the C_2C_3 time-of-flight measurements. The output of the linear mixer for the C_1C_3 time-of-flight measurement was also recorded in a pulse

Fig. 13.--Sample time-of-flight spectra showing the deuteron, proton, and pion peaks, the latter two scaled by a factor of 1000. The time separation between the peaks corresponds to a flight path of 58 ft. Five channels correspond to 1 nsec.

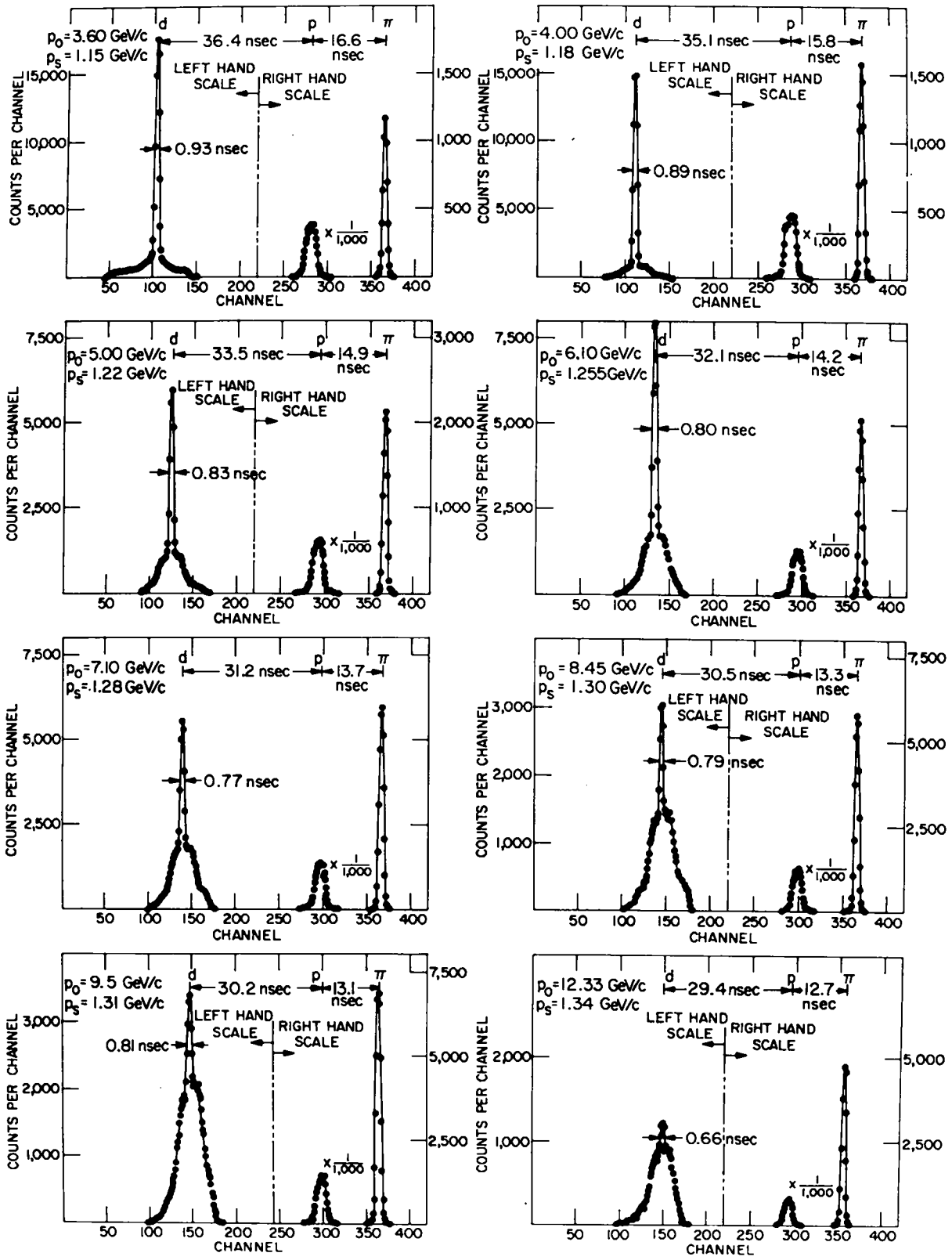
p_0=3.60 GeV/c
p_s = 1.15 GeV/c
d
36.4 nsec
p
16.6 nsec
π
LEFT HAND SCALE
RIGHT HAND SCALE
0.93 nsec
COUNTS PER CHANNEL
CHANNEL
p_0=4.00 GeV/c
p_s= 1.18 GeV/c
35.1 nsec
15.8 nsec
0.89 nsec
p_0=5.00 GeV/c
p_s= 1.22 GeV/c
33.5 nsec
14.9 nsec
0.83 nsec
p_0=6.10 GeV/c
p_s= 1.255GeV/c
32.1 nsec
14.2 nsec
0.80 nsec
p_0=7.10 GeV/c
p_s=1.28 GeV/c
31.2 nsec
13.7 nsec
0.77 nsec
p_0 = 8.45 GeV/c
p_s = 1.30 GeV/c
30.5 nsec
13.3 nsec
0.79 nsec
p_0= 9.5 GeV/c
p_s= 1.31 GeV/c
30.2 nsec
13.1 nsec
0.81 nsec
p_0=12.33 GeV/c
p_s=1.34 GeV/c
29.4 nsec
12.7 nsec
0.66 nsec
x 1/1,000

Fig. 13.

height analyzer (PHA) which was gated by an S123D unscaled and an S123P scaled. As expected, this "balanced TAC" technique proved superior to simply ORing the upper and the lower tubes together before sending them to the overlap mixer, a possibility explored during the experiment.

Figure 13 shows sample time-of-flight spectra as recorded in the PHA for incident proton momentum p_o = 3.6 to 12.3 GeV/c. These spectra are for the total flight path of 58 ft. The proton and pion peaks, scaled by a factor of 1000, appear on the right and the deuterons on the left. The sharp deuteron peak, corresponding to deuterons from reaction (1), has an average full width at half maximum (FWHM) over many runs of 0.8 $\pm$ 0.1 nsec. It is superimposed on a broad distribution due to non-hydrogen background. The sharpness of the peak is due to the fact that the experiment was performed in the flat region of the $p_d\theta_d$ diagram of reaction (1) where p_d is almost constant (see Figure 2).

The outputs of the linear mixers were also sent to two pairs of differential discriminators, one pair of which was set to accept only deuterons (F123D) and the other pair only protons (F123P). The TV and spark chambers were triggered by an S123D. For the range of spectrometer momentum covered in this experiment, the deuteron-proton time-of-flight difference varied from 14.7 to 18.4 nsec for the 29 ft flight path, and the S123D was more than adequate to separate out the deuterons. However, the F123D with its

superior resolution was available for higher spectrometer momenta. The total delay from the passage of a particle through C_3 until an S123D signal was available in the electronics trailer was about 300 nsec.

A glycerol threshold Čerenkov counter, whose dimensions were 12 in. x 12 in. x 2-1/4 in. was placed at the end of the spectrometer after C_3. With a refractive index of 1.473, the minimum momentum for the production of Čerenkov radiation in glycerol is 0.13 GeV/c for pions, 0.87 GeV/c for protons, and 1.73 GeV/c for deuterons. In the momentum range 1.14 to 1.34 GeV/c, the rejection efficiency of the Čerenkov counter was measured and found to be 97% for pions, 70% for protons, and 8% for deuterons. The Čerenkov counter was gated by C_3 at the local logics, eventually strobed by a deuteron event, and placed on magnetic tape for future cross checking of the identification of deuterons by time-of-flight. The Čerenkov counter was not used in the initial electronic selection of events.

Gating and Dead Time

The logics were gated to count only during the flat portion of the ZGS "front porch." This was accomplished in part using signals made available to the experimenter from the ZGS control room. These included, among others: a start pulse synchronized with the ZGS cycle, a signal in phase with and proportional to the ZGS field, and clock

pulses for timing purposes. The ZGS field signal, the integrated counts from one of the monitor M_2 counters, and the output of a gate generator were simultaneously displayed on a storage oscilloscope as shown in Figure 6. The oscilloscope provided a visual display of the ZGS field and the position of the beam spill and gating pulse relative to that field. By adjusting the start and stop pulses to the gate generator, the spill-gating of the logics could be visually set.

In order to reduce multiple tracks in the chambers, a pile-up gate requirement was placed on the events. The "singles" counts from time-of-flight counter C_1 were fed to the input of a pile-up gate which generated a continuously updated gating level until 1 μsec had lapsed between particles in C_1. This gating level blocked the events which could give multiple tracks. The number of these varied from a few per cent to as much as 40% of the events.

The television system, the spark chambers, and the electronic circuitry were all subject to an insensitive period or dead time, following activitation, during which they could not accept further tasks. The actual TV dead time was 8 msec and will be discussed in the next section. However, because of spark chamber deterioration it was found best not to run the spark chambers much faster than 60 Hz. Therefore, the TV-spark chamber dead time was set at 15 msec per event by a gate generator. The dominating sources

of dead time in the electronic circuitry were the time-to-amplitude converters and the "singles" counts in the time-of-flight counters. The TAC's had a dead time of 10 μsec which was fixed by a gate generator. The pulses from the local logics for counters C_1, C_2, and C_3 were lengthened from 10 nsec to 50 nsec in the initial stages of the time-of-flight circuitry. The discriminator circuits used for lengthening the pulses had a dead time of twice the pulse width or 100 nsec in this case. The output of the TAC dead time gate generator and the 50 nsec pulses from C_1, C_2, and C_3 were combined to form an electronic dead time veto signal.

All gating and dead time loses were monitored and recorded throughout the experiment. The TV-spark chamber dead time losses were accounted for by counting monitor M_1 before and after application of the TV-spark chamber dead time gate. The pile-up gate losses were accounted for by counting the number of events (S123D) before and after application of the pile-up gate. Finally, the electronic dead time was accounted for by counting monitor M_1 before and after application of the electronic dead time veto signal. The quantities discussed above, plus many others required for data reduction or control of the experiment, were displayed on 100 MHz scalers and recorded photographically at the end of each run.

Spark Chambers and Vidicon Readout

The spark chambers with automatic vidicon readout were essentially the same as those used in an earlier experiment at the ZGS[17] and described elsewhere.[18] However, primarily in order to handle a higher event rate, several changes were made to the system, of which the most significant included: the reduction of the number of scanning lines per view from 30 to 8, the reading of the chambers in parallel rather than serially, and the inclusion of a buffer memory between the digitizer and the magnetic tape unit. The buffer memory was required so that the magnetic tape unit, with its relatively slow mechanical drive, would not limit the number of events recorded per ZGS pulse. In the new arrangement the magnetic tape unit was activated only between ZGS pulses and then received the full contents of the buffer memory.

The 10 in. x 10 in. spark chambers had six 0.3 in. gaps consisting of seven planes of 1/2 mil aluminum foil.

---

[17] H. L. Anderson, S. Fukui, D. Kessler, K. A. Klare, M. V. Sherbrook, H. J. Evans, R. L. Martin, E. P. Hincks, N. K. Sherman, and P. I. P. Kalmus, Phys. Rev. Letters 18, 89 (1967).

[18] H. L. Anderson and A. Barna, Rev. Sci. Instr. 35, 492 (1964); E. P. Hincks, H. L. Anderson, H. J. Evans, S. Fukui, D. Kessler, K. A. Klare, J. W. Lillberg, M. V. Sherbrook, R. L. Martin, and P. I. P. Kalmus, Proceedings of the 1966 International Conference on Instrumentation for High Energy Physics, Stanford, 1966, p. 63.

The chambers were operated at about 10 kV. The gas mixture (90% neon, 10% helium) was flowed continuously through the chambers at about 5 cc/sec and exhausted to the atmosphere after passing through an oxygen analyzer. The chambers were pulsed using EG & G high voltage pulsers (HV100) and hydrogen thyratrons (HY10). The total delay from the time a particle passed through C_3 until the chambers were pulsed was about 570 nsec. This included: the 300 nsec delay in forming the triggering pulse (S123D) mentioned earlier, 50 nsec cable delay from the electronics trailer to the HV100 at the local logics, 50 nsec delay through the HV100, 20 nsec cable delay from the local logics to the spark chambers, and about 150 nsec delay in the hydrogen thyratron at the spark chambers. A constant 15 V clearing field was maintained on the chambers to sweep away residual electrons. In order to increase the spark chamber memory time for good events, a coincidence between C_1 and C_2, timed for deuterons only, was formed at the local logics to turn off the clearing field on all chambers in about 50 nsec from the time a deuteron passed through C_2.

Figure 14 shows a spark chamber with its optical system for imaging both orthogonal views on one vidicon. The system utilized a series of first-surface mirrors and 90° bends to direct both spark chamber views to the camera lens, one above the other. In addition, there was a field lens, beam splitter, and fiducial pattern associated with

Fig. 14.--Spark chamber and optical system for imaging both orthogonal views on one vidicon.

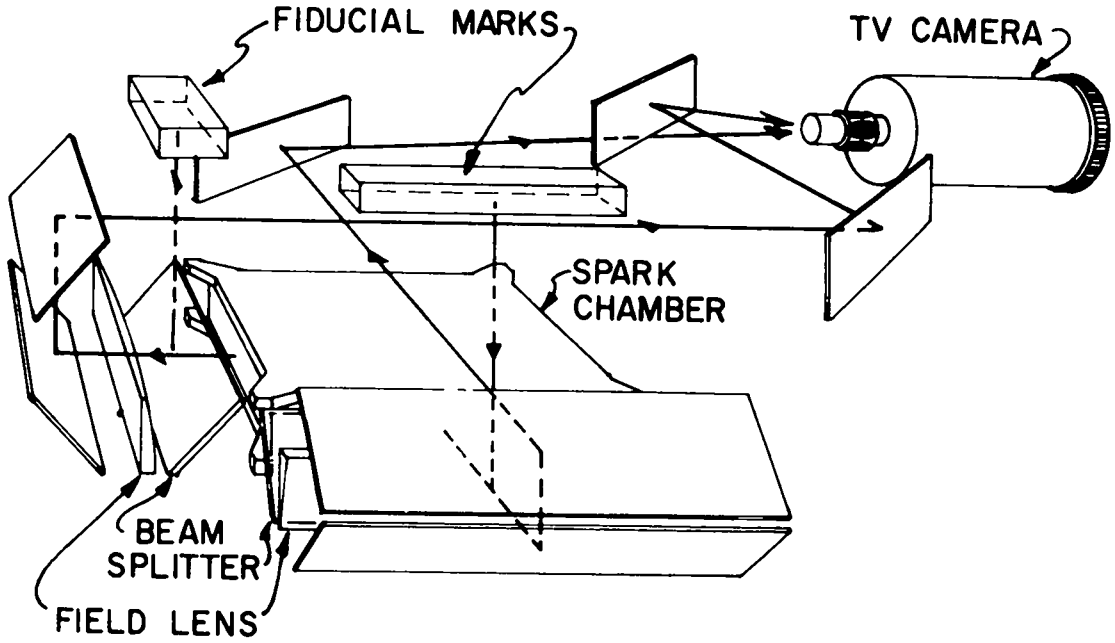
FIDUCIAL MARKS
TV CAMERA
SPARK CHAMBER
BEAM SPLITTER
FIELD LENS

Fig. 14.

each view. The fiducial pattern consisted of a mask with a series of crosses and parallel slits illuminated with light from incadescent lamps, which could be switched on when needed. The beam splitters were partially aluminized 1/4 in. glass plates, set at 45° to both the spark chamber and the fiducial pattern. The beam splitters served to reflect some of the light from the fiducial marks (about 40% from the first surface) into the optical system. They also wasted about half the light from the sparks, but this was manageable. The fiducial patterns were accurately located with respect to the housing which contained the spark chamber and optical system. Data taking was interrupted about every 1/2 hour or 5000 events and the fiducial marks recorded on the magnetic tape in the same manner as the particle tracks.

The spark chamber readout system could handle up to eight television cameras and consisted of a TV monitor, a digitizer, a magnetic core storage buffer, a magnetic tape unit, and a storage display tube readout. The system had a capacity of four sparks per chamber with an indication of overflow if more than four sparks occurred. Each view was digitized eight times and with two views per camera and up to eight cameras a total of 128 words of memory per event was required. The buffer storage unit was a Nanomemory 900 with a capacity of 8,192 sixty-five bit words. Therefore, the memory had a potential capacity of sixty-four events per ZGS beam spill.

The television system was a modified closed circuit system utilizing a twenty-one line non-interlaced frame. The horizontal sweep was 62.5 μsec per line. The vertical period was 1.31 msec and the aspect ratio was approximately 2 to 5. Five lines were used for vertical retrace and sixteen lines for digitization of the spark images. All eight cameras were driven in parallel by the digitizer using signals derived from the countdown circuitry of a 20 MHz clock. After the vidicon signal passed through a zero-crossing circuit, the spark image was digitized by sequentially stopping the first of four scalers which had simultaneously started counting pulses from the 20 MHz clock at the beginning of the scan line. There were 1024 addresses per line so that each address corresponded to about 1/4 mm in real space for 10 in. spark chambers. Additional sparks would stop the second, third, and fourth scalers.

During horizontal fly-back eight words were serially read into the buffer memory. Each word consisted of forty-four bits from the four digitizing scalers, eight bits of auxiliary data, and seven flag bits. With 128 words per event the system could handle 36 seven-decade BCD auxiliary data devices. Auxiliary data included: clock time, run number, event number, hodoscope information, Čerenkov counter identification, time-of-flight, digital voltmeter readings of magnet currents, and all scaler quantities necessary for the proper normalization of the data. At the

end of a beam spill the accumulated data was read from the memory and written on magnetic tape using IBM compatible format at a density of 556 bits per in. at a rate of 62,500 characters per sec. The read head of the tape unit was coupled to a reconstructor which could display a single event on a storage display tube. This device served as an overall system monitor. The TV dead time, including four frames for erasing the vidicons, was about 8 msec. However, as noted earlier, the dead time was set at 15 msec, thus limiting the system to a maximum of thirty-three events in a 500 msec beam spill. Typically, with 10^{11} protons/pulse about fifteen to twenty-five events were recorded in a 500 msec spill. It took about two to three hours to fill a magnetic tape with 30,000 events. This included: time for writing fiducial marks on the magnetic tape, recording data, changing tapes, and filling or emptying the hydrogen target.

CHAPTER III

ANALYSIS

Processing of Magnetic Tapes

The magnetic tapes were processed on the University of Chicago IBM-7094/7040 and the Los Alamos Scientific Laboratory CDC-6600 computers. The fiducial marks and spark chamber tracks were reconstructed by a pattern recognition program from the digitized coordinates on magnetic tape. The fiducial pattern was used to establish a third order relation between the digitized vidicon output and coordinates in real space. The quadratic term in this expression was found to be small and due to non-linearities in the spark chamber optics and TV horizontal sweep. The calibration was updated about every 5000 events, a procedure which was found by experience more than adequate to compensate for small long term drifts in the vidicon system.

The analysis program required at least one track in at least three of the five spark chambers, one of which had to be either SC_1 or SC_2. Events which did not meet the above criteria were rejected. The program kept a record of all rejected events and the reason for rejection. The category of "three or more chambers missing" comprised a

spark chamber or vidicon inefficiency.

For events fulfilling the criteria for acceptance, the momentum determination program fitted a trajectory through the spark chambers, computed the goodness of fit (χ^2), and computed the deuteron momentum from the calculated curvature in the second bending magnet. Since the trajectory was over-determined with four spark chambers, the accuracy with which the spatial coordinates of the tracks were measured could be determined and was found to be about $\pm$ 0.4 mm. This uncertainty includes: the 1/4 mm resolution in the digitization of the sparks, drifts in the vidicon system, multiple Coulomb scattering between the spark chambers, and magnetic field fluctuations.

The magnetic field of the two bending magnets was set and periodically checked with a Varian F-8A, NMR fluxmeter. In addition, the digital voltmeter (DVM) readings of the current in the quadrupoles and bending magnets were recorded on the magnetic tape with each ZGS pulse. To save computer time, the momentum determination program was designed to employ a nominal value of the magnetic field, except when the measured field deviated significantly from the nominal field in which case the actual field calculated from the DVM readings was used. It was found that, throughout most of the experiment, the power supplies to the bending magnets were extremely stable and that the nominal value of the fields as set by the NMR was sufficiently accurate.

This technique introduced an uncertainty of about $\pm$ 0.1% in the magnetic fields.

Events with a poor χ^2 in either the horizontal (X) or vertical (Y) planes were classified as accidental coincidences and rejected. Events with too many solutions (good χ^2) in X were classified as ambiguous and considered a spectrometer analysis inefficiency.

The program retraced the trajectory back through the first bending magnet and the quadrupole pair to the target and computed the angle of emission. Trajectories that did not come from the target region were classified as non-hydrogen events and rejected. The target, as seen on a retrace scatter plot, appears larger than its actual dimensions due to multiple scattering, magnetic field uncertainties, and momentum measuring errors. Because of a very favorable signal-to-background ratio for reaction (1), the target region for accepted events was liberally chosen as $\pm$ 12 cm in the horizontal direction and $\pm$ 8 cm in the vertical direction. Due principally to multiple scattering (0.02 radiation length, primarily from the scintillator of C_1) the angle of emission could only be determined to within $\pm$ 2 mrad. This is, however, considerably less than the angular spread of the incident beam at the target. The errors in the angle measurement, moreover, have little effect upon the mass resolution due to the flatness of the kinematic lines in the region investigated. The program

Fig. 15.--Sample missing-mass squared spectra in the pion region. The upper (circles) and lower (crosses) spectra show the target-full and target-empty data, respectively, normalized to the same number of incident protons.

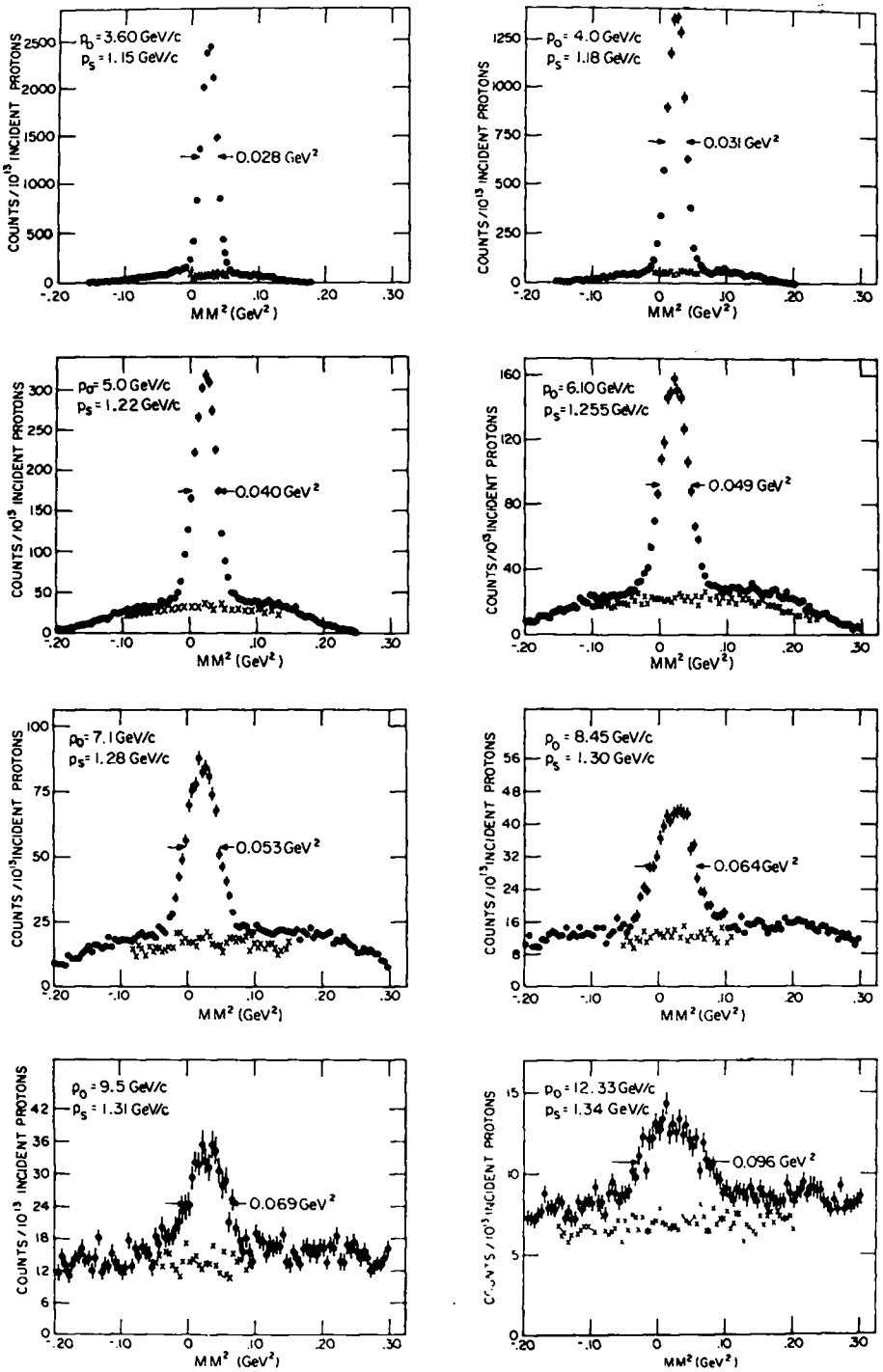
p_0 = 3.60 GeV/c
p_s = 1.15 GeV/c
0.028 GeV²
p_0 = 4.0 GeV/c
p_s = 1.18 GeV/c
0.031 GeV²
p_0 = 5.0 GeV/c
p_s = 1.22 GeV/c
0.040 GeV²
p_0 = 6.10 GeV/c
p_s = 1.255 GeV/c
0.049 GeV²
p_0 = 7.1 GeV/c
p_s = 1.28 GeV/c
0.053 GeV²
p_0 = 8.45 GeV/c
p_s = 1.30 GeV/c
0.064 GeV²
p_0 = 9.5 GeV/c
p_s = 1.31 GeV/c
0.069 GeV²
p_0 = 12.33 GeV/c
p_s = 1.34 GeV/c
0.096 GeV²
COUNTS / 10^{13} INCIDENT PROTONS
MM² (GeV²)

Fig. 15.

corrected for the energy loss of the deuteron in the spectrometer and computed the missing-mass squared (MM^2). Since the position of the vertex in the target is indeterminate, the program could not correct for the energy loss of the deuteron in the target.

While providing the important MM^2 distribution, the computer output presented considerable additional information necessary for the proper control of the experiment, maintenance of equipment, and analysis of the results. The program provided raw fiducial data, sample events with kinematical quantities, χ^2 distributions, momentum and angular distributions, time-of-flight distributions, X and Y distributions at the target, collimator and spark chambers, hodoscope distributions, and phase space distributions. Besides considerable information not mentioned, the program also provided the event rejection categories and the scaler data for normalization. Although not used for the study of reaction (1), the program was capable of placing additional selection criteria on the events, such as, hodoscope, time-of-flight, or Čerenkov requirements.

Figure 15 presents sample missing-mass squared spectra in the pion region for incident proton momentum in the range p_o = 3.6 to 12.3 GeV/c. As indicated in Figure 15, the experimentally measured spectrometer resolution (FWHM) in missing-mass squared, $\delta(MM^2)$, increases from 0.028 GeV^2 at 3.6 GeV/c to 0.096 GeV^2 at 12.3 GeV/c. A

calculation of $\delta(MM^2)$, including the uncertainties from the incident proton momentum and angle, the uncertainty due to the energy loss of the deuteron in the target, and the deuteron momentum and angle measurement errors, yields a FWHM of 0.030 GeV^2 at 3.6 GeV/c and 0.102 GeV^2 at 12.3 GeV/c in good agreement with the experimentally observed values. The momentum measuring error (about $\pm$ 1/3%) was the single largest contributor to the uncertainty in the missing-mass and was usually about twice the contribution from the energy loss of the deuterons in the target.

The peak in the missing-mass squared spectra centered at 0.02 GeV^2 is clearly due to deuterons from reaction (1). The background, indicated by the target empty points, comes from the target walls and the radiation shield. An additional background effect, which is evident above and below the $d\pi^+$ peak, comes from deuterons produced in the walls of the vacuum pipe by secondary particles from the hydrogen in the target. Accidental coincidences simulating deuterons do not appear to contribute to the spectra. Accidental coincidences between the C_1C_3 and C_2C_3 time-of-flight measurements were counted during the experiment and found to be negligible.

Normalization and Summation of Spectra

To obtain the differential cross section for reaction (1) from the missing-mass spectra, it was necessary to normalize each run to the M_1 monitor, make the corrections for spectrometer inefficiencies and logic dead time, and correct the spectra for the spectrometer momentum acceptance as calculated by the Monte-Carlo program and shown in Figure 9. This made it possible to add spectra taken at the same incident momentum p_o but different settings of the spectrometer. The number of corrected events $\Delta\nu_f(\Delta\nu_e)$ for the target full (empty) lying within a given bin of the missing-mass squared histogram was calculated from the formula

$$\Delta\nu_f(\Delta\nu_e) = \frac{G_f(G_e)}{\epsilon_\alpha\epsilon_\beta\epsilon_\gamma\epsilon_\delta\epsilon_\varepsilon M_1}$$

where

$G_f(G_e)$ = the number of events in a given bin of the missing-mass squared histogram for the target full (empty) and passing all criteria of the event analysis program

ϵ_α = the combined efficiency of the spark chambers and vidicon cameras

ϵ_β = the spectrometer analysis efficiency due to the ambiguity of events with too many good solutions in the horizontal plane

ϵ_γ = the correction for the pile-up gate losses

ε_δ = the correction for the electronic dead time losses

ε_ε = the spectrometer efficiency over the accepted momentum interval as calculated by the Monte-Carlo program (including the estimated loss of deuterons to multiple scattering)

M_1 = the total number of Monitor M_1 counts recorded after application of the TV-spark chamber dead time gate.

The spectrometer efficiencies ε_α and ε_β were computed for each run from the event rejection categories and were typically 0.995 and 0.98, respectively. The pile-up gate efficiency ε_γ, the electronic dead time correction ε_δ, and the M_1 monitor counts were computed form the appropriate auxiliary data for each run. Both ε_γ and ε_δ were strongly rate dependent and varied greatly from run to run depending upon the EPB intensity and whether the target was full or empty. Consequently, ε_γ ranged from 0.60 to 0.95 and ε_δ from 0.90 to 0.99. Finally, the usable portion of the spectra was restricted to the region where the spectrometer efficiency ε_ε was at least 40% that of the central value. This permitted a momentum acceptance of about $\pm$ 4%.

Because of the slightly larger non-hydrogen background present during the target full runs, the target empty runs were normalized to the target full runs in the non-physical region (negative missing-mass squared) and then subtracted.

What remains is a prominent peak due to single pion production superimposed on a contribution due to multipion production, slowly rising with energy. In our preliminary analysis[1] of the data we simply drew the background by eye as a straight line fit to the data above and below the peak, and ascribed to single pion production the sum total of events in the peak above the straight line. Subsequently, we analyzed the data above the pion peak in much more detail. For several values of our incident momentum we took a complete missing-mass spectrum up to $MM^2 = 1.6$ GeV^2. This enabled us to make a more detailed evaluation of the multipion contribution. The data above the pion peak was dominated by a broad maximum due to ρ production on a smoothly rising background which we took to be the contributions according to phase space of 2π, 3π, and $\pi\rho$ production. The analysis of this part of the data will be described in a subsequent publication. We mention it here because we used it to make a more accurate subtraction of the multiparticle background under the pion peak. After this subtraction we obtained good fits of the pion peak with a Gaussian distribution, the integral of which gave the event rate ν.

The refined analysis had an inappreciable effect on the cross sections for low values of p_o, where the background was quite small in any case. The new background subtraction gave cross sections which were generally higher but by less than 5% except for the values at $p_o = 6.20$, 6.85, 7.90, 8.45, 9.00, 11.00, and 12.33 GeV/c, where the increases were by 6.4, 6.5, 22.8, 7.4, 6.6, 6.3, and 23.7 percent, respectively.

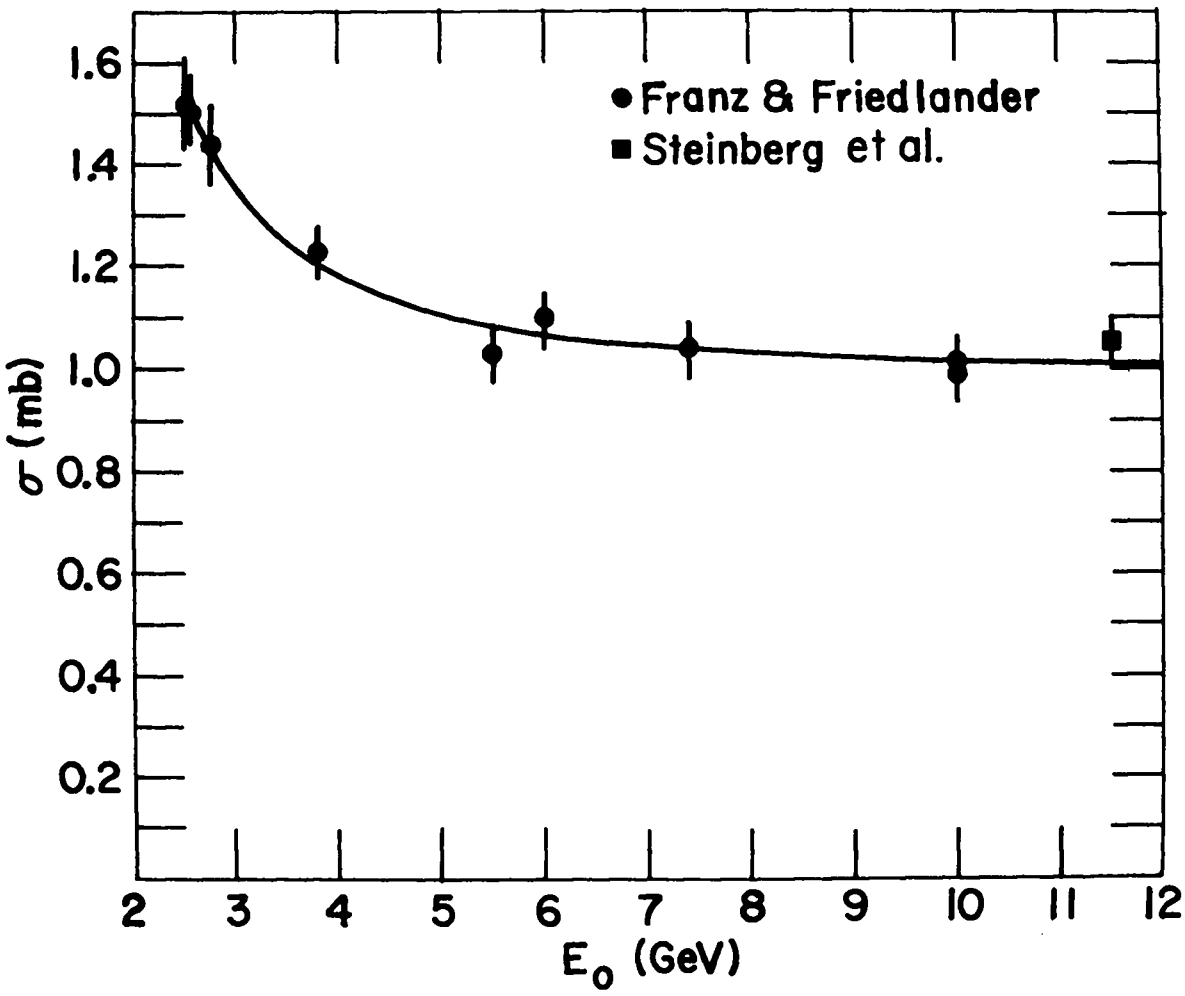

Fig. 16.--Cross section for production of the α-branch of Tb^{149} from Au by proton bombardment as a function of incident proton kinetic energy E_o. The curve represents a least squares fit to the data of Ref. 14 (square) and Ref. 19 (circles).

Calibration of Monitor M_1

It was noted earlier that the M_1 monitor counts were related to the number of incident protons by gold foil activation. A calibration run consisted of exposing a 6 in. x 6 in. x 1/2 mil foil at the SEM_2 stand for about four hours while the experiment was in progress. During the bombardment, the total number of monitor M_1 counts, the time of exposure, and any changes in relative intensity of the EPB were recorded. A radioautograph of the foil was taken after exposure to determine the beam size at the SEM_2 stand and the proper cutting pattern of the foil. About four hours after the end of the foil exposure the α particles were counted in a calibrated windowless flow-type proportional counter. The number of protons Q, incident upon the foil, was calculated from this measurement and the know cross section σ for the production of the α-branch of Tb^{149} from Au. Figure 16 shows the cross section σ as a function of proton kinetic energy E_o. The curve shown is a least squares fit to the data of Franz and Friedlander[19] for the range of proton energies of interest in this experiment and to the one point of Steinberg et al.[14] at 11.5 GeV. There is a $\pm$ 5% normalization uncertainty in these data which is not included in the errors of our differential cross sections for reaction (1).

---

[19] E. M. Franz and G. Friedlander, Nucl. Physc. 76, 123 (1966).

At least one gold foil was exposed at most of the EPB momenta studied in this experiment and thirteen calibrations were made at 12.3 GeV/c providing a good check on the internal consistency of the measurements. The reproducibility of the calibrations depended to a great extent upon the foils receiving scrupulous attention and handling from initial bombardment to final counting of the α particles. This required keeping an accurate log of the exposure time and any relative changes in the EPB intensity. Since for counting purposes the foils were not to exceed about 1 in. sq., the large beam size at the SEM_2 stand (up to 4 in. in diameter) required a rather complex cutting pattern of the exposed foil. This in turn generated a great number of foil sections which had to be meticulously cut, mounted, and electrically grounded to metal disks. Deviations from the established procedure resulted in very unreliable measurements. Also, the large beam size at SEM_2 made it difficult to collect all the protons in the EPB. Figure 17 shows the ratio M_1/Q versus p_o for all calibrations taken during the experiment; also shown is the least squares fit that was made to these data. From the internal consistency of the 12.3 GeV/c points, we obtain an error of $\pm$ 3.4% in our calibration.

Fig. 17.--Ratio of monitor M_1 counts to the number of incident protons M_1/Q as a function of incident proton momentum p_o. The protons were counted using the intact gold foil technique (see Ref. 14). The curve is a least squares fit to all calibrations taken during the experiment.

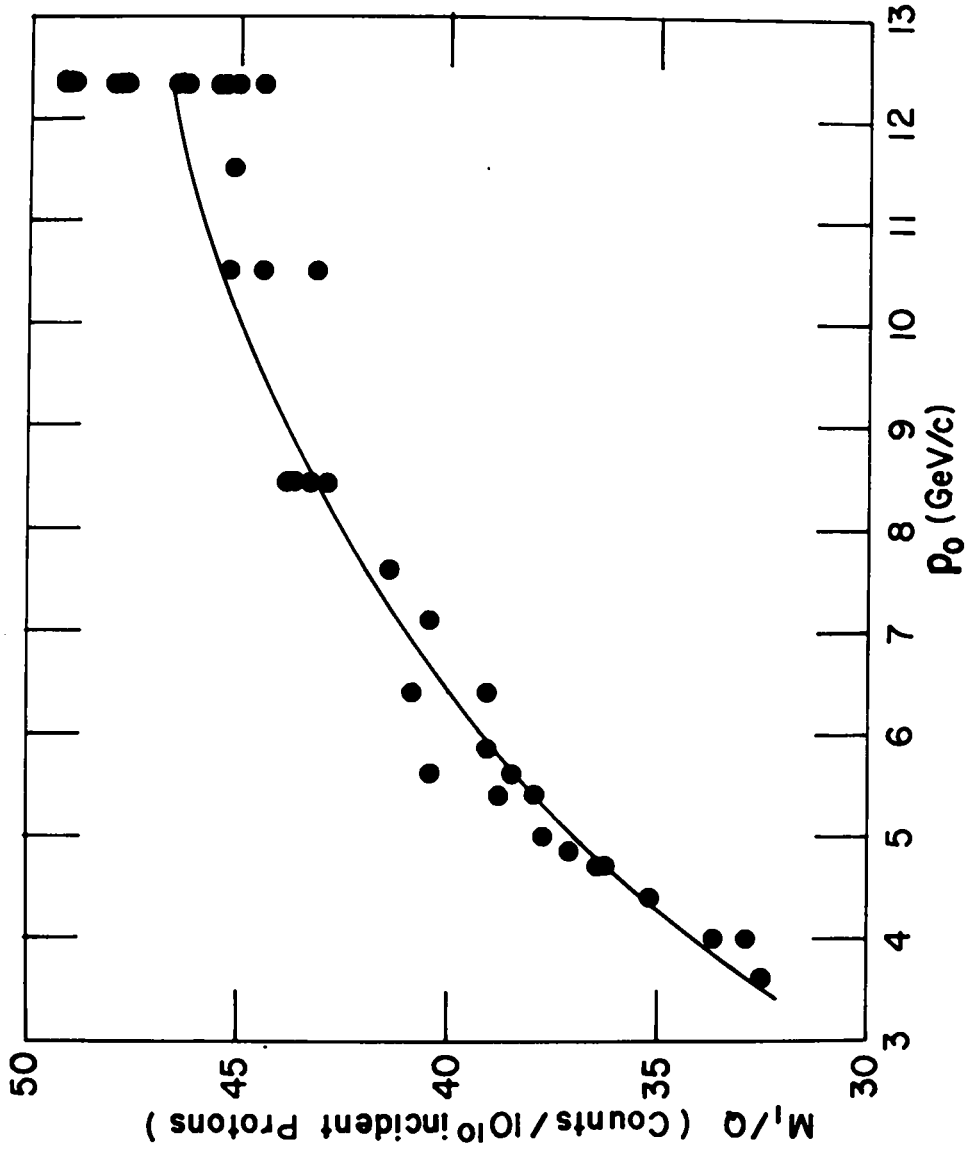
50
45
40
35
30
3
4
5
6
7
8
9
10
11
12
13
M_1/Q (Counts / 10^{10} incident Protons)
P_0 (GeV/c)

Fig. 17.

CHAPTER IV

CORRECTIONS TO DATA

Residual Hydrogen Gas

Target full and target empty runs were taken at each measurement of the differential cross section and the background removed by subtraction. A correction was applied for the residual H_2 gas in the empty target. A definite warming effect of the target was noted during target empty runs (about 1 h) from the decrease of the M_2 rate with time. This decrease, about 2-4% of the target empty effect, was due to the decrease of the H_2 gas density with rising temperature. The target empty temperature was assumed to be $35 \pm 15^{\circ}K$, giving a net H_2 gas effect of $1.1 \pm 0.5\%$ of the liquid H_2 effect.

Target Diameter

Since the H_2 target was a vertical cylinder, most of the proton beam did not traverse a diameter. Therefore, the target diameter was averaged over a horizontal beam width of 2.5 ± 0.5 cm. This resulted in a correction reducing the diameter by a factor of 0.980 ± 0.008.

Proton Beam Attentuation

There was a slight attentuation of the proton beam in traversing the hydrogen target. An effective target diameter d_{eff} was defined by integrating the beam intensity over the actual diameter using the relation

$$d_{eff} = \int_0^d e^{(\rho\, \sigma_{p-p})x}\, dx$$

where

d = the actual target diameter = 7.43 cm

ρ = the density of liquid hydrogen = 4.23×10^{22} protons/cm^3

σ_{p-p} = the total p-p cross section = 42 mb.

The total p-p cross section changes very little over the range of incident proton momentum covered in this experiment and 42 mb is a good average value.[20] Since the EPB intensity was measured downstream of the hydrogen target, the above considerations resulted in a correction increasing the beam intensity by a factor of 1.007.

Deuteron Losses

Deuterons were lost by multiple Coulomb scattering and nuclear interactions. As mentioned earlier, the Monte-Carlo program was used to estimate the amount of multiple

---

[20] D. V. Bugg, A. J. Oxley, J. A. Zoll, J. G. Rushbrooke, V. E. Barnes, J. B. Kinson, W. P. Dodd, G. A. Doran, and L. Riddiford, Phys. Rev. 133, B1017 (1964).

scattering within the spectrometer. It was found that the correction to be applied ranged from 0.953 ± .005 at the lowest spectrometer momentum to 0.987 ± .005 at the highest. An estimate of the deuteron loss due to nuclear interactions can be made from a knowledge of the amount and type of material in the deuteron path (hydrogen target, helium, air, mylar windows, counters, and spark chambers) and from the deuteron-nucleon cross section σ_{dN}. The cross section for the various absorbers was approximated by $\sigma_{dA} = \sigma_{dN} A^{2/3}$ where σ_{dN} ranges from 74 mb at the lowest deuteron momentum of interest to 62 mb at the highest.[21] This resulted in a transmission probability which ranged from 0.953 to 0.959 ± 0.010.

Counting Efficiency

The over-all counting efficiency ϵ_e was defined to include the detection efficiency of the time-of-flight counters, the dead time of the zero-crossing discriminators at the local logics, and the 3 of 6 veto rate at the local logics. The detection efficiency of the counters was measured using protons and pions in the spectrometer beam. Two trigger counters (1 in. sq.) were placed on opposite sides of the time-of-flight counter to be studied and the efficiency

---

[21] F. F. Chen, C. P. Leavitt, and A. M. Shapiro, Phys. Rev. 103, 211 (1956).

determined as a function of position. An estimate of the dead time in counter C_1 was made by assuming an average of 10^5 particles/pulse in C_1 and an average beam spill of 500 msec. During the experiment, the 3 of 6 veto rate in counter C_1 was continuously recorded and 2.9% found to be a good average value. The dead time and 3 of 6 veto rate in counter C_2 were estimated from a knowledge of the relative counting rates in C_1 and C_2. The dead time in C_3 was negligible and C_3 had no 3 of 6 veto. The over-all counting efficiency was calculated from the relation

$$\varepsilon_e = \prod_{i=1}^{7} \varepsilon_i$$

where

ε_1 = the detection efficiency of C_1 = 0.998

ε_2 = the detection efficiency of C_2 = 0.998

ε_3 = the detection efficiency of C_3 = 1.000

ε_4 = the efficiency due to dead time in the zero-crossing discriminator of C_1 at the local logics = 0.997

ε_5 = the efficiency due to dead time in the zero-crossing discriminator of C_2 at the local logics = 0.999

ε_6 = the efficiency due to the 3 of 6 veto in C_1 = 0.971

ε_7 = the efficiency due to the 3 of 6 veto in C_2 = 0.993.

The over-all counting efficiency was found to be $\varepsilon_e = 0.96 \pm 0.02$. The relatively large uncertainty is due primarily to the dependence of the dead time and 3 of 6 veto effect upon the EPB rate.

CHAPTER V

RESULTS

The differential cross section for reaction (1) in the c.m. system was calculated from the formula

$$\left(\frac{d\sigma}{d\omega}\right)_{c.m.} = \frac{\nu}{(Q/M_1)\ \rho\ d\ (d\omega/d\Omega)\ \Delta\Omega\ \varepsilon_a\ \varepsilon_b\ \varepsilon_c\ \varepsilon_d\ \varepsilon_e}$$

where

ν = the number of events in the pion peak as obtained from the analysis program

Q/M_1 = the number of protons traversing the target normalized to monitor M_1

ρ = the density of liquid hydrogen = 4.23×10^{22} protons/cm^3

d = the diameter of the target = 7.43 ± 0.08 cm

$d\omega/d\Omega$ = the solid angle transformation from the laboratory to the c.m. system

$\Delta\Omega$ = the laboratory solid angle of the spectrometer = 2.08×10^{-4} sr

ε_a = the correction for the residual hydrogen gas in the target = 0.989 ± 0.005

ε_b = the correction to the target diameter = 0.980 ± 0.008

ε_c = the correction for the attentuation of the proton beam in the target = 1.007

ε_d = the transmission probability of deuterons due to nuclear interactions = 0.953 to 0.959 $\pm$ 0.010 depending on momentum

ε_e = the counting efficiency = 0.96 $\pm$ 0.02.

With the exception of the counting efficiency ε_e which is rate dependent, the uncertainties in the corrections listed above introduce systematic errors in the differential cross sections. When combined quadratically with the $\pm$ 5% uncertainty in the cross section for the production of Tb^{149} α particles in gold, they yield a $\pm$ 5.3% normalization error in our differential cross sections. The nonstatistical error in the relative differential cross sections arises from a $\pm$ 0.8% error in the laboratory to center-of-mass transformation due to the uncertainty in the beam energy, the $\pm$ 2% uncertainty in the counting efficiency ε_e, and the $\pm$ 3.4% uncertainty in the gold foil calibration. These errors, when combined quadratically, contribute $\pm$ 4.1% to the error in the differential cross sections for reaction (1). These differential cross sections in the c.m. system, obtained from the missing-mass spectra, are presented in Table 1. The uncertainties shown are compounded from the $\pm$ 4.1% error and the statistical error, but they do not include the $\pm$ 5.3% normalization error.

TABLE I

MEASURED CENTER-OF-MASS DIFFERENTIAL CROSS SECTION FOR THE REACTION $p + p \rightarrow d + \pi^+$.

p_o [a] (GeV/c)	p_d [b] (GeV/c)	$\cos\theta_{c.m.}$	s [c] (GeV^2)	$(d\sigma/d\omega)_{c.m.}$ [d] ($\mu b/sr$)
3.40	1.140	0.9928	8.38	14.96 ± 0.67
3.60	1.154	0.9934	8.74	13.57 ± 0.58
3.85	1.169	0.9940	9.20	11.72 ± 0.48
4.00	1.177	0.9943	9.47	10.44 ± 0.48
4.40	1.197	0.9950	10.20	6.68 ± 0.29
4.70	1.210	0.9954	10.75	4.74 ± 0.22
4.85	1.216	0.9956	11.03	3.87 ± 0.17
5.00	1.221	0.9957	11.31	3.47 ± 0.15
5.15	1.226	0.9959	11.58	3.05 ± 0.14
5.35	1.233	0.9961	11.96	2.76 ± 0.13
5.60	1.241	0.9963	12.42	2.65 ± 0.13
5.85	1.248	0.9965	12.88	2.50 ± 0.12
6.00	1.252	0.9966	13.16	2.63 ± 0.16
6.10	1.254	0.9967	13.34	2.51 ± 0.12
6.20	1.257	0.9967	13.53	2.48 ± 0.16
6.30	1.259	0.9968	13.72	2.51 ± 0.16
6.40	1.261	0.9969	13.90	2.40 ± 0.13
6.85	1.271	0.9971	14.73	2.12 ± 0.22
7.10	1.276	0.9972	15.20	1.62 ± 0.09
7.35	1.280	0.9973	15.66	1.50 ± 0.18
7.60	1.285	0.9974	16.13	1.47 ± 0.08
7.90	1.290	0.9976	16.69	1.40 ± 0.21
8.45	1.297	0.9977	17.71	1.15 ± 0.06
9.00	1.305	0.9979	18.74	0.922 ± 0.066
9.50	1.310	0.9980	19.67	0.864 ± 0.078
10.50	1.320	0.9982	21.54	0.664 ± 0.063
11.00	1.324	0.9983	22.48	0.558 ± 0.062
11.50	1.328	0.9984	23.41	0.491 ± 0.058
12.33	1.335	0.9985	24.96	0.433 ± 0.047

[a] p_o is the laboratory momentum of the incident proton.

[b] p_d is the laboratory momentum of the deuteron.

[c] s is the square of the total energy in the center-of-mass.

[d] A normalization error of ±5.3% has not been incorporated in the differential cross sections.

As was noted earlier, the differential cross sections could also be extracted from the time-of-flight data, corresponding to a pure counter experiment. This was possible for reaction (1) because of the very favorable signal-to-background ratio, which is evident in the typical time-of-flight spectra shown in Figure 13. The differential cross sections were computed from the time-of-flight data using only the target full runs. The only deuterons present in the time-of-flight spectra originating from the liquid hydrogen are those of reaction (1). Therefore, the background was subtracted from the time-of-flight spectra by fitting a quadratic relation to the non-hydrogen deuterons in a selected region above and below the sharp peak corresponding to deuterons from reaction (1). This was found to be more reliable than either a linear fit or a subtraction of target empty runs. The over-all agreement between the time-of-flight and missing-mass cross sections was very good with most measurements agreeing within a few per cent. A few of the high momentum points showed individual deviations as high as 19%; however, in this region the time-of-flight signal-to-background ratio is far less favorable and these large deviations are probably due to the uncertainties in the time-of-flight background subtraction.

CHAPTER VI

DISCUSSION

The differential cross sections for the process $p + p \rightarrow d + \pi^+$ obtained in this experiment are given in tabular form in Table 1. The values listed here differ only in minor ways from those used for the plot given in our original publication.[1] Here we give the incident proton laboratory momentum p_o, the laboratory momentum of the observed deuteron (central value) p_d, and the cosine of the center-of-mass production angle corresponding to the fixed 5^o (central value) laboratory angle at which the deuteron was observed. We give the square of the c.m. energy, and finally, the differential cross section in the c.m. system. As a function of incident momentum, our cross sections decrease more rapidly at first from a high of 15.0 μb/sr at 3.4 GeV/c, flatten off at 2.5 μb/sr around 6.0 GeV/c, and then decrease rather regularly for higher values of incident momentum. At our highest momentum, 12.3 GeV/c, the cross section has fallen to 0.43 μb/sr. In contrast, the elastic channel in p-p collisions has differential cross sections in the forward direction which increase over the range of incident momenta covered here.

Fig. 18.--Forward ($\cos\theta_{c.m.} = 1$) differential cross section for the reaction $p + p \rightarrow d + \pi^+$ in the c.m. system as a function of incident proton laboratory momentum p_o and total energy in the c.m. $E_{c.m.}$, including previously published work (Refs. 7-11, 22-27). All data shown was either measured directly at $\cos\theta_{c.m.} = 1$, extrapolated to $\cos\theta_{c.m.} = 1$ from a measured angular distribution of the form $a + b \cos^2\theta_{c.m.}$, or extrapolated to $\cos\theta_{c.m.} = 1$ using the relation $e^{-p_\perp / b}$ where $p_\perp$ is the transverse momentum in GeV/c and b varies between 0.26 and 0.19 GeV/c (see Ref. 23). The curve is from a calculation of the one-pion-exchange contribution according to the model of Yao.

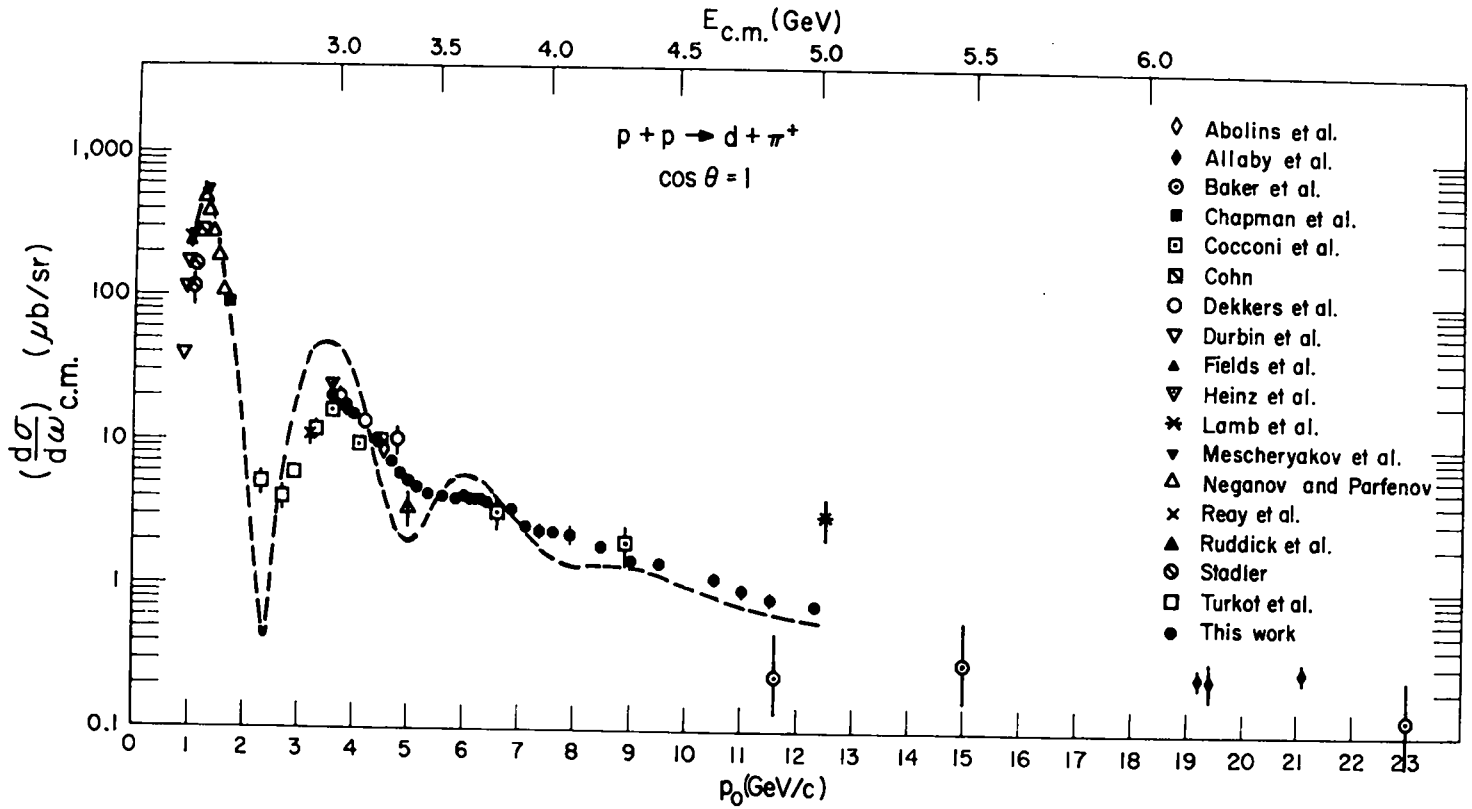
$E_{c.m.}$ (GeV)
3.0
3.5
4.0
4.5
5.0
5.5
6.0
$p + p \rightarrow d + \pi^+$
$\cos\theta = 1$
$(\frac{d\sigma}{d\omega})_{c.m.}$ (μb/sr)
1,000
100
10
1
0.1
0 1 2 3 4 5 6 7 8 9 10 11 12 13 14 15 16 17 18 19 20 21 22 23
p_0(GeV/c)
Abolins et al.
Allaby et al.
Baker et al.
Chapman et al.
Cocconi et al.
Cohn
Dekkers et al.
Durbin et al.
Fields et al.
Heinz et al.
Lamb et al.
Mescheryakov et al.
Neganov and Parfenov
Reay et al.
Ruddick et al.
Stadler
Turkot et al.
This work

Fig. 18.

At 12.3 GeV/c, the p-p elastic scattering cross section for the same momentum transfer is 80 mb/sr, some 2×10^5 times greater than in the d π^+ channel.

The general behavior of the cross section becomes more apparent when our data are combined with those of other measurements. Three peaks are evident. The first is well known and has a sharp maximum at $p_o = 1.25$ GeV/c ($E_{c.m.} = 2.17$ GeV). There is a second pronounced maximum at $p_o = 3.5$ GeV/c ($E_{c.m.} = 3.0$ GeV). The third peak doesn't show a clear maximum but there is a definite shoulder centered at $p_o = 6.3$ GeV/c ($E_{c.m.} = 3.7$ GeV). Beyond this energy further peak structure, if any, appears to be even more strongly damped. The cross section decreases rather smoothly up to $p_o = 22.9$ GeV/c ($E_{c.m.} = 6.7$ GeV/c) the highest energy measured to date.[22]

These features are displayed in Figure 18 where we have attempted to extrapolate the cross section obtained near the forward direction to 0^o. In carrying out this program, we made use of the relation

$$\left(\frac{d\sigma}{d\omega}\right)_{c.m.} = \left(\frac{d\sigma}{d\omega}\right)_o e^{-p_\perp/b} \qquad (2)$$

---

[22] W. F. Baker, E. W. Jenkins, A. L. Read, A. D. Krisch, J. Orear, R. Rubinstein, D. B. Scarl, and B. T. Ulrich, Phys. Rev. 136, B779 (1964).

found by Allaby et al.[23] to give a good fit to the data at 21.1 GeV/c and at 3.62 GeV/c. Here $p_\perp$ is the transverse momentum in GeV/c. The parameter b seems to be somewhat energy dependent. According to Allaby et al.,[23] it is equal to 0.26 GeV/c for the data of Heinz et al.[9] at $E_{c.m.} = 3.0$ GeV and to 0.19 GeV/c for their own data at $E_{c.m.} = 6.4$ GeV. In the absence of more precise information, we used values of b varying linearly with $E_{c.m.}$ between these two values.

Plotted in Figure 18 are all available c.m. differential cross sections[7-11,22-26] for the reaction $p + p \rightarrow d + \pi^+$ at 0°, for $E_{c.m.} > 2.3$ GeV either as measured directly or extrapolated using (2). Table II gives a tabulation of all experimental data on reaction (1) and its inverse for $E_{c.m.} > 2.3$ GeV. In the region $2.3 < E_{c.m.} < 3.0$ GeV, the angular distribution, as measured both by Dekkers et al.[8]

---

[23] J. V. Allaby, F. Binon, A. N. Diddens, P. Dritiel, A. Klovning, R. Meunier, J. P. Peigneux, E. J. Sacharidis, K. Schlüpmann, M. Spighel, J. P. Stroot, A. M. Thorndike, and A. M. Wetherell, Phys. Letters 29B, 198 (1969).

[24] R. C. Lamb, R. A. Lundy, T. B. Novey, D. D. Yovanovitch, and R. Lander, Phys. Rev. Letters 17, 100 (1966).

[25] K. Ruddick, L. G. Ratner, K. W. Edwards, C. W. Akerlof, R. H. Hieber, and A. D. Krisch, Phys. Rev. 165, 1442 (1968).

[26] N. W. Reay, A. C. Melissinos, J. T. Reed, T. Yamanouchi, and L. C. L. Yaun, Phys. Rev. 142, 918 (1966); M. A. Abolins, R. Graven, R. McCarthy, G. A. Smith, L. H. Smith, A. B. Wicklund, R. L. Lander, and D. E. Pellet, to be published.

TABLE II

MEASUREMENTS OF DEUTERON PRODUCTION IN THE REACTION $p + p \rightarrow d + \pi^+$ FOR TOTAL CENTER-OF-MASS ENERGY ABOVE 2.3 GeV.

Reference	θ [a]	$E_{c.m.}$ [b] (GeV)
Chapman et al.[c]	90 to 156°	2.3
Heinz et al.[d]	90 to 165°	2.3 to 3.0
Dekkers et al.[e]	90 to 172°	2.5 to 3.3
Reay et al.[f]	180°	2.8
Turkot et al.[g]	0°	2.5 to 2.9
present work[h]	87 mrad	2.9 to 5.0
Cocconi et al.[i]	60 mrad	3.0 to 4.3
Abolins et al.[i]	0°	3.0, 3.2
Ruddick et al.[k]	90°	3.4
Baker et al.[l]	56°	4.9
	43°	5.5
	35°	6.7
Lamb et al.[m]	0°	5.0
Allaby et al.[n]	40 mrad	6.15
	25 mrad	6.2
	12 to 60 mrad	6.4

[a] Angle of emission of the deuteron with respect to the incident proton direction. Angles expressed in degrees are in the center-of-mass system. Angles expressed in milliradians are in the laboratory system.

[b] Total energy in the center-of-mass system.

[c] K. R. Chapman, T. W. Jones, Q. H. Khan, J. S. C. McKee, H. B. Van Der Raay, and Y. Tanimura, Phys. Letters 11, 253 (1964).

[d] R. M. Heinz, O. E. Overseth, D. E. Pellet, and M. L. Perl, Phys. Rev. 167, 1232 (1968).

[e] Measured the inverse reaction $\pi^+ + d \rightarrow p + p$. D. Dekkers, B. Jordan, R. Mermod, C. C. Ting, G. Weber, T. R. Willits, K. Winter, X. DeBouard, and M. Vivargent, Phys. Letters 11, 161 (1964).

[f] N. W. Reay, A. C. Melissinos, J. T. Reed, T. Yamanouchi, and L. C. L. Yuan, Phys. Rev. 142, 918 (1966).

[g] F. Turkot, G. B. Collins, and T. Fujii, Phys. Rev. Letters 11, 474 (1963).

[h] Detected the deuterons emitted backward in the center-of-mass system.

[i] Detected the deuterons emitted forward in the center-of-mass system. G. Cocconi, E. Lillethun, J. P. Scanlon, C. A. Stahlbrandt, C. C. Ting, J. Walters, and A. M. Wetherell, Phys. Letters 7, 222 (1963).

[j] M. A. Abolins, R. Graven, R. McCarthy, G. A. Smith, L. H. Smith, A. B. Wicklund, R. L. Lander, and D. E. Pellet, to be published.

[k] K. Ruddick, L. G. Ratner, K. W. Edwards, C. W. Akerlof, R. H. Hieber, and A. D. Krisch, Phys. Rev. 165, 1442 (1968).

[l] W. F. Baker, E. W. Jenkins, A. L. Read, A. D. Krisch, J. Orear, R. Rubinstein, D. B. Scarl, and B. T. Ulrich, Phys. Rev. 136, B779 (1964).

[m] R. C. Lamb, R. A. Lundy, T. B. Novey, D. D. Yovanovitch, and R. Lander, Phys. Rev. Letters 17, 100 (1966).

[n] Detected the deuterons emitted forward in the center-of-mass system. J. V. Allaby, F. Binon, A. N. Diddens, P. Dritiel, A. Klovning, R. Meunier, J. P. Peigneux, E. J. Sacharidis, K. Schlupmann, M. Spighel, J. P. Stroot, A. M. Thorndike, and A. M. Wetherell, Phys. Letters 29B, 198 (1969).

(who measured the inverse reaction) and by Heinz et al.,[9] is changing very rapidly near 0° making the extrapolation rather uncertain. Therefore, in this energy interval the data of Dekkers and Heinz, and one point from the present work have not been shown. For $E_{c.m.} \geq 3.0$ GeV equation (2) was assumed to hold. Also shown are sufficient data[27] below $E_{c.m.} = 2.3$ GeV to give a proper indication of the maximum at $E_{c.m.} = 2.17$ GeV. In this region the angular distribution of reaction (1) (and its inverse) has a simple $a + b \cos^2\theta_{c.m.}$ dependence so that the extrapolation to 0° could be made reliably. It is interesting to note that with these deletions, all data in the region $2.3 < E_{c.m.} < 6.7$ appear to be consistent. Even the very high transverse momentum data of Baker et al.[22] and Ruddick et al.[25] seem to fall on a smooth curve once the extrapolation to 0° is carried out according to equation (2). The one point of Lamb et al.[24] at $E_{c.m.} = 5.0$ GeV is in marked disagreement with what otherwise is a consistent set of points. Lamb et al.[24] identified reaction (1) by measuring the momentum

---

[27] R. Durbin, H. Loar, and J. Steinberger, Phys. Rev. 84, 581 (1951); T. H. Fields, J. G. Fox, J. A. Kane, R. A. Stallwood, and R. B. Sutton, Phys. Rev. 95, 638 (1954); H. I. Stadler, Phys. Rev. 96, 496 (1954); C. E. Cohn, Phys. Rev. 105, 1582 (1957); M. G. Mescheryakov, B. S. Neganov, N. P. Bogachev, and V. M. Sidorov, Dokl. Akad. Nauk SSSR 100, 673 (1955); M. G. Mescheryakov and B. S. Neganov, Dokl. Akad. Nauk SSSR 100, 677 (1955); B. S. Neganov and L. B. Parfenov, Zh. Eksperim. i Teor. Fiz. 34, 767 (1958) [English transl.: Soviet Phys. - JETP 7, 528 (1958)].

of pions emitted at 180° and requiring the missing-mass to be the deuteron. We have no ready explanation why this type of measurement should appear to overestimate the cross section by such a large factor. We have deleted this point in the analysis that follows.

Some years ago Orear[28] fitted the differential cross sections for reaction (1) using the following empirical formula

$$\left(\frac{d\sigma}{d\omega}\right)_{c.m.} = A\,(s/s_o)^a\, e^{-p_\perp/b}$$

where $s_o = 1\ \text{GeV}^2$, s is the total c.m. energy squared in GeV^2, and $p_\perp$ is the transverse momentum in GeV/c. He took a = -1 and determined A = 0.12 mb/sr and b = 0.16 GeV/c. This relation gave a reasonable fit to the data at high energy and high transverse momentum, but it failed to predict the correct behavior of the differential cross section at high energy and low momentum transfer. At $E_{c.m.} = 5$ GeV it gives a forward differential cross section which is too large by an order of magnitude. Using all the available data for $E_{c.m.} > 3.9$ GeV, we redetermined the parameters in the Orear formula and obtained

$$A = 2.60 \pm 0.71 \text{ mb/sr}$$

$$a = -2.5 \pm 0.1$$

$$b = 0.20 \pm 0.01 \text{ GeV/c}.$$

---

[28] J. Orear, Phys. Letters 13, 190 (1964).

The fit, which includes 23 data points, has a χ^2 per degree of freedom of 0.80. These data have been plotted in Figure 19 to show the s dependence of the cross section in the high energy region. The forward differential cross section is seen to fall off like $s^{-2.5}$.

The appearance of three peaks at 2.17, 3.0, and at 3.7 GeV, center-of-mass energy, suggests a connection with the first three resonances in $\pi^+ p$ elastic scattering. These are the first three T = 3/2 nucleon isobars at M_Δ = 1.236, 1.950, and 2.420 GeV. The connection was first pointed out by Chahoud, Russo, and Selleri[29] following the discovery of the second peak in reaction (1) by Cocconi et al.[11] This follows easily from the one-pion-exchange model (Figure 20a) and is due to the fact that the binding of n and p into a deuteron fixes the kinematics of the three body intermediate state with the following relationship

$$s' = \frac{1}{2}(s - M^2 + \mu^2) + m^2 \qquad (3)$$

where s is the square of the c.m. energy for reaction (1), $s' = M_\Delta^2$ is the invariant mass of the πN vertex, and M, m, and μ are the deuteron, nucleon, and pion masses, respectively. This formula neglects the deuteron binding energy and the momentum distribution of the bound nucleons, but

---

[29] J. Chahoud, G. Russo, and F. Selleri, Phys. Rev. Letters 11, 506 (1963).

Fig. 19.--Differential cross section for the reaction $p + p \rightarrow d + \pi^+$ in the c.m. system. The function $e^{p_\perp/b}(d\sigma/d\omega)_{c.m.}$ is plotted against the total energy squared in the c.m. ($s = E^2_{c.m.}$) for $E_{c.m.} > 3.9$ GeV, including previously published work (Refs. 11, 22-23). The curve shown is the result of fitting the experimental data with a function of the form $A(s/s_o)^a e^{-p_\perp/b}$ where s_o is taken as 1 GeV^2 and the parameters from the fit are found to be $A = 2.60 \pm 0.71$ mb/sr, $a = -2.5 \pm 0.1$, and $b = 0.20 \pm 0.01$ GeV/c.

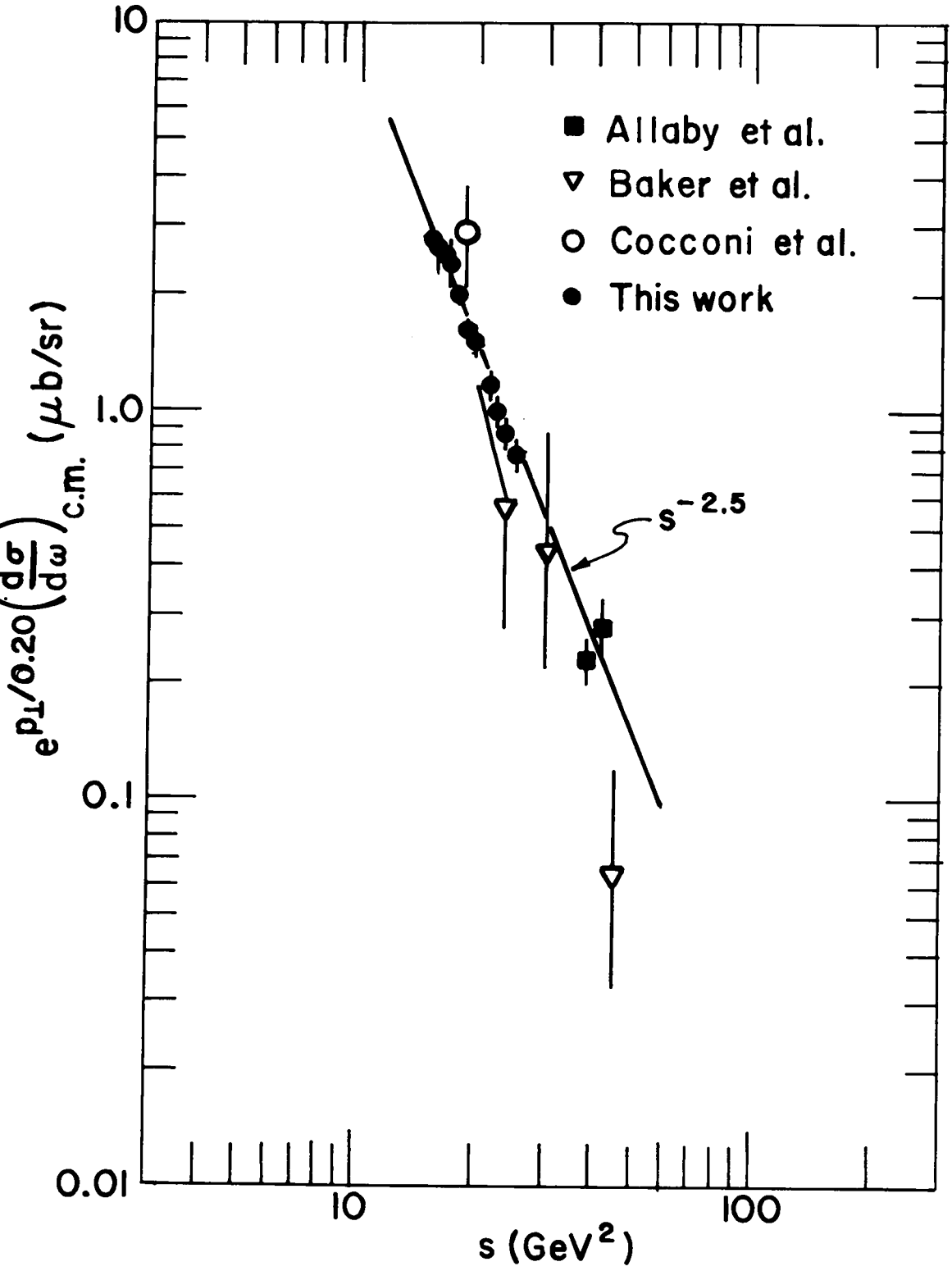
10
1.0
0.1
0.01
10
100
s (GeV²)
e^{p_T/0.20}(dσ/dω)_{c.m.} (μb/sr)
Allaby et al.
Baker et al.
Cocconi et al.
This work
s^{-2.5}

Fig. 19.

Fig. 20.--Feynman diagrams for the reaction $p + p \rightarrow d + \pi^+$ proceeding via (a) one-pion-exchange with the exchange of either a π^+ or a π^o meson, (b) one-nucleon-exchange, and (c) the formation of a dibaryon resonance in the direct channel.

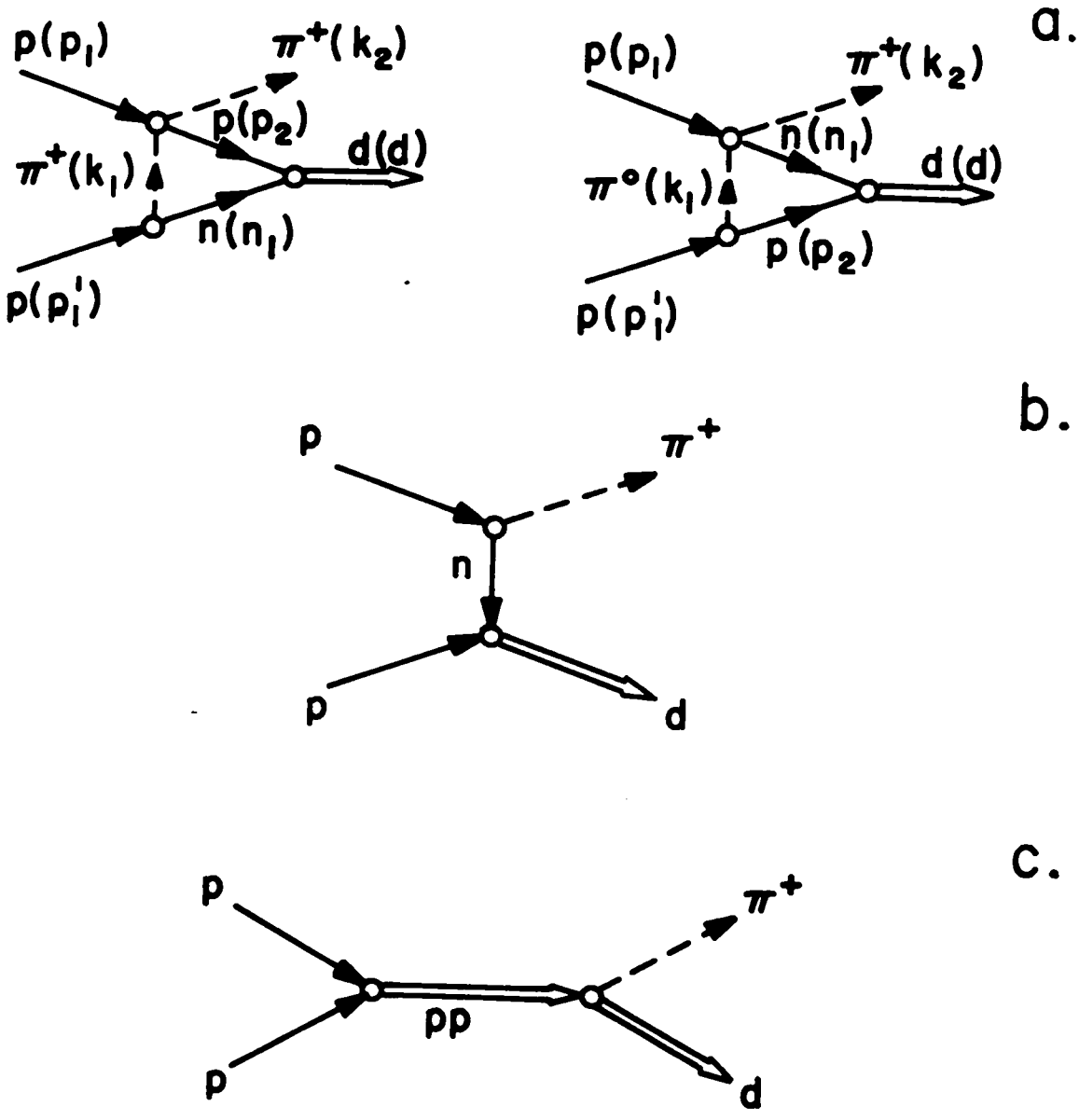
a.
p(p1)
π+(k2)
p(p2)
d(d)
π+(k1)
n(n1)
p(p1')
p(p1)
π+(k2)
n(n1)
d(d)
π°(k1)
p(p2)
p(p1')
b.
p
π+
n
p
d
c.
p
π+
pp
p
d

Fig. 20.

these can be shown to have only a minor effect on the validity of (3). Equation (3) predicts peaks at $E_{c.m.} = 2.19$, 3.06, and 3.67 GeV, in close correspondence with the observed maxima. No other peaks appear, supposedly a consequence of the isopin structure of the one-pion-exchange diagram. This predicts that other peaks such as those corresponding to the T = 1/2 isobars, would be suppressed by a factor of 16 compared to the T = 3/2 isobars.

These aspects, and the success of the one-pion-exchange model in the interpretation of pion production in p-p collisions, among other reactions, in the 1-2 GeV region, led Yao[30] to attempt a more complete calculation of the $d\pi^+$ production. In Yao's formulation the matrix elements which appear in the calculation are evaluated in terms of the $\pi^{\pm}p$ elastic and charge exchange scattering cross sections in the following form

$$\frac{d\sigma}{d\omega}(s,\theta) = G(s,\theta)\left[3\frac{d\sigma^{+}}{d\omega_{\pi}} - \frac{d\sigma^{-}}{d\omega_{\pi}} + 3\frac{d\sigma^{o}}{d\omega_{\pi}}\right] + (p_1 \rightleftarrows p'_1) \qquad (4)$$

Here, $G(s,\theta)$ is a slowly varying function of the square of the c.m. energy s, θ is the angle between the incoming proton and the outgoing deuteron in the center-of-mass, $0 \leq \theta \leq \pi/2$,

---

[30] T. Yao, Phys. Rev. 134, B454 (1964).

and $d\sigma/d\omega_\pi$ are the differential πp scattering cross sections, evaluated at their c.m. energy squared s' (Equation 3) and their c.m. scattering angle θ'.

The function $G(s,\theta)$ is entirely determined from other experiments and contains such factors as the pion-nucleon coupling constant $G^2/4\pi$, the deuteron form factor, as well as the Ferrari-Selleri off-the-mass-shell correction function, as given in Yao's paper.[30]

The second term in equation (4) is obtained from the first term by interchanging p_1 and p'_1 (see Figure 20a). This interchange amounts to changing $\cos\theta$ to $-\cos\theta$. The four-momentum squared, k_1^2, of the exchanged virtual pion is given by

$$-k_1^2 = -2m^2 + \frac{1}{4}(s + M^2 - \mu^2) - dp\cos\theta$$

where p and d are the three-momenta in the c.m. of the incoming proton and outgoing deuteron, respectively, θ is as defined in equation (4), and s, M, m, and μ are as defined in equation (3). For $\cos\theta = 1$, $\cos\theta' = -1$ and $-k_1^2$ is a minimum. From this it follows that backward πp scattering is very important for deuteron formation in the forward direction. It is by backward emission of the π^+ at the upper vertex (see Figure 20a) that the nucleon momentum may be reversed in direction and made equal to that of the nucleon emerging from the lower vertex after emitting a pion with small k_1. The factor $G(s,\theta)$ is a maximum in this case.

Fig. 21.--Backward differential cross section in the c.m. system for (a) $\pi^+ p$ elastic scattering, (b) $\pi^- p$ elastic scattering, and (c) $\pi^- p$ charge exchange scattering as a function of incident pion laboratory momentum p_π. It should be noted that the variable $E_{c.m.}$ does not refer to the total energy in the c.m. of the πp system but to the total energy in the c.m. of the reaction $p + p \rightarrow d + \pi^+$. The two systems have been related through the Yao model as discussed in the text. The data are from a survey of the literature (see Ref. 31). The curves are hand fits to the data.

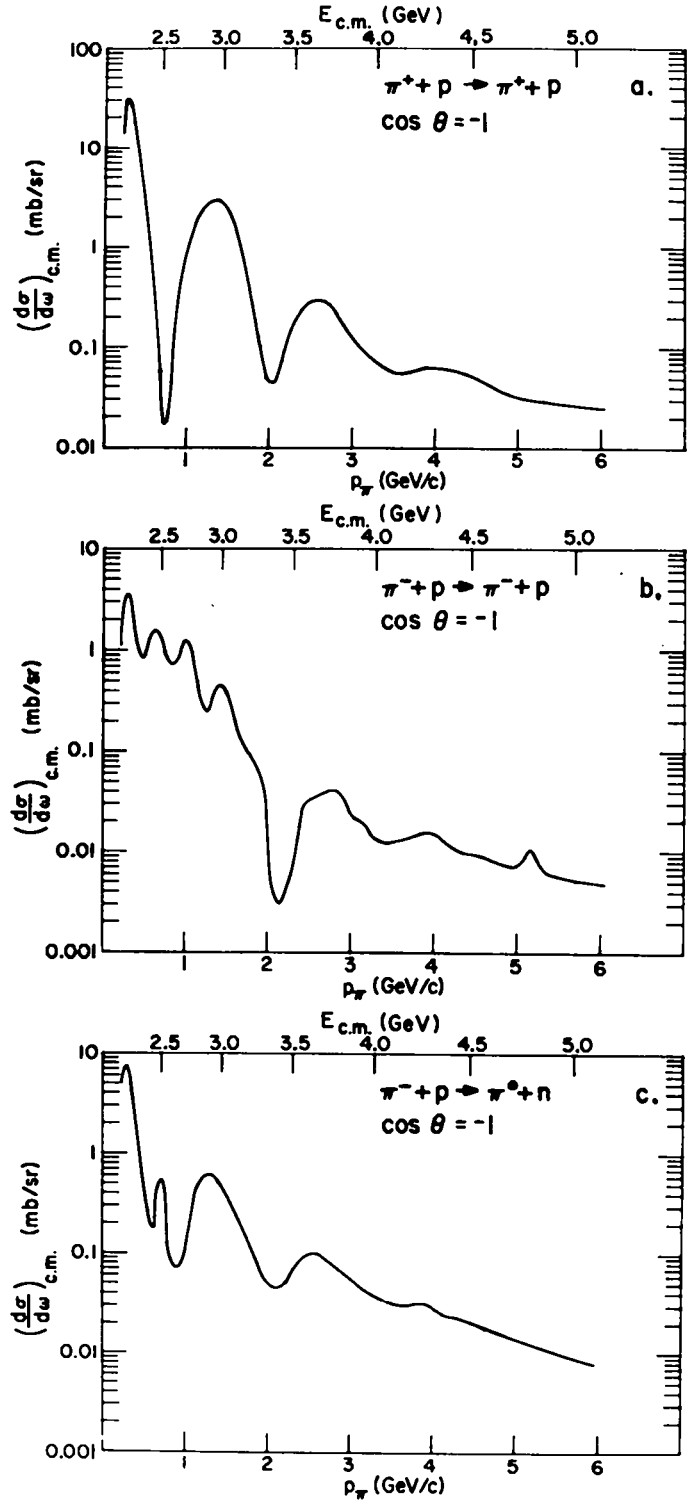
E c.m. (GeV)
2.5 3.0 3.5 4.0 4.5 5.0
π⁺ + p → π⁺ + p
a.
cos θ = -1
(dσ/dω)c.m. (mb/sr)
100
10
1
0.1
0.01
1 2 3 4 5 6
p_π (GeV/c)
E c.m. (GeV)
2.5 3.0 3.5 4.0 4.5 5.0
π⁻ + p → π⁻ + p
b.
cos θ = -1
(dσ/dω)c.m. (mb/sr)
10
1
0.1
0.01
0.001
1 2 3 4 5 6
p_π (GeV/c)
E c.m. (GeV)
2.5 3.0 3.5 4.0 4.5 5.0
π⁻ + p → π⁰ + n
c.
cos θ = -1
(dσ/dω)c.m. (mb/sr)
10
1
0.1
0.01
0.001
1 2 3 4 5 6
p_π (GeV/c)

Fig. 21.

Fig. 22.--Forward differential cross section in the c.m. system for (a) π^+p elastic scattering, (b) π^-p elastic scattering, and (c) π^-p charge exchange scattering as a function of incident pion laboratory momentum p_π. It should be noted that the variable $E_{c.m.}$ does not refer to the total energy in the c.m. of the πp system but to the total energy in the c.m. of the reaction $p + p \rightarrow d + \pi^+$. The two systems have been related through the Yao model as discussed in the text. The data are from a survey of the literature (see Ref. 31). The curves are hand fits to the data.

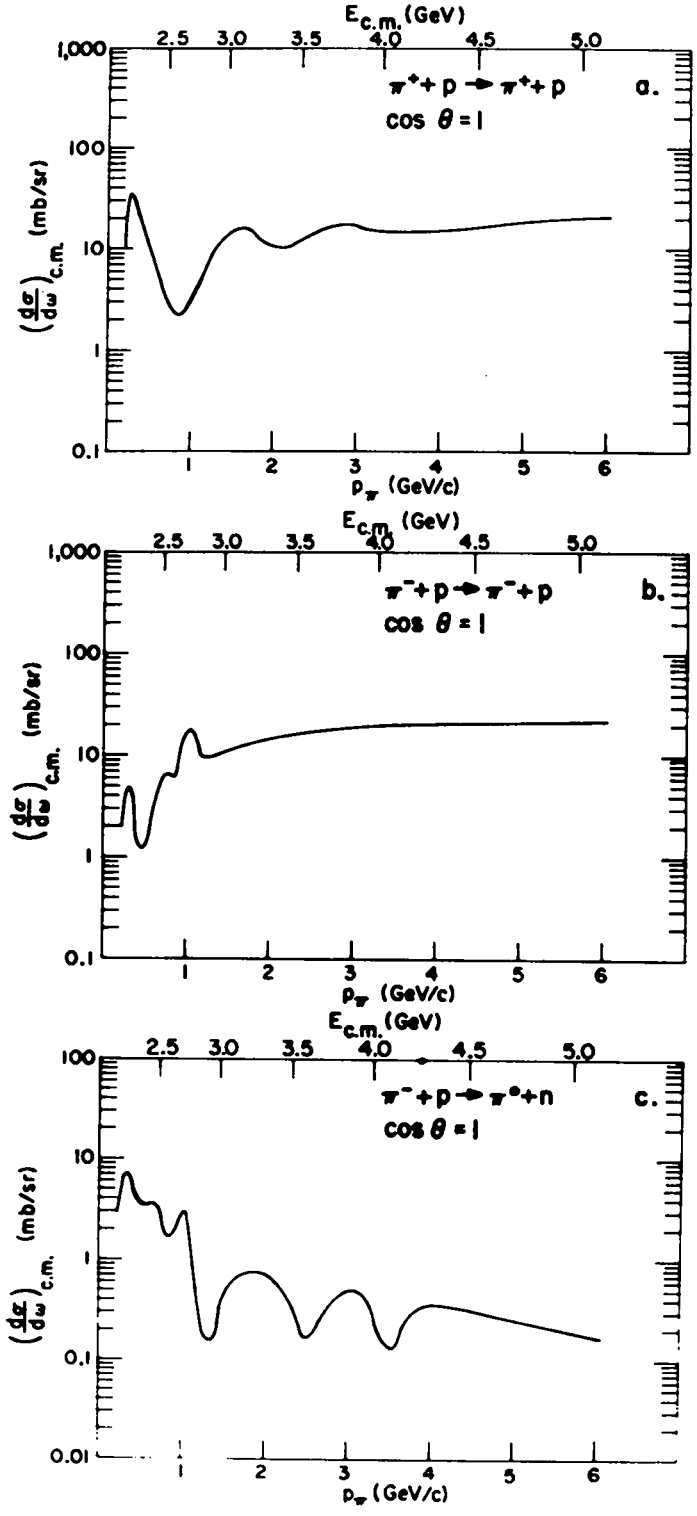
E c.m. (GeV)
2.5 3.0 3.5 4.0 4.5 5.0
1,000
100
10
1
0.1
π⁺ + p → π⁺ + p
a.
cos θ = 1
(dσ/dω) c.m. (mb/sr)
1 2 3 4 5 6
p_π (GeV/c)
E c.m. (GeV)
2.5 3.0 3.5 4.0 4.5 5.0
1,000
100
10
1
0.1
π⁻ + p → π⁻ + p
b.
cos θ = 1
(dσ/dω) c.m. (mb/sr)
1 2 3 4 5 6
p_π (GeV/c)
E c.m. (GeV)
2.5 3.0 3.5 4.0 4.5 5.0
100
10
1
0.1
0.01
π⁻ + p → π⁰ + n
c.
cos θ = 1
(dσ/dω) c.m. (mb/sr)
1 2 3 4 5 6
p_π (GeV/c)

Fig. 22.

The contribution of the second term corresponds to $\cos\theta = -1$, $\cos\theta' = 1$. In this case $-k_1^2$ is very large, the exchanged virtual pion is very far from the mass shell, and the one-pion-exchange approximation becomes highly dubious. The value of $G(s,\theta)$ will be small but since forward πp scattering cross sections are quite large, the second term can make an appreciable, albeit questionable, contribution.

Equation (4) neglects the interference between the two contributions. This appeared to be unimportant in the calculation of the low energy behavior. Here, we take the interference into account by writing

$$\frac{d\sigma}{d\omega} = |T_1|^2 + |T_2|^2 + 2T_1T_2\cos\phi$$

where $|T_1|^2$ and $|T_2|^2$ correspond to the two terms in (4). The relative phase ϕ may range from full constructive interference ($\cos\phi = +1$) to full destructive interference ($\cos\phi = -1$). The leeway allowed by the uncertainty in the phase turns out to be quite large, amounting as it does to a decade or so in the high energy region. The curve given in Figure 18 was calculated for $\cos\phi = 0$, corresponding to the incoherent sum. This curve was calculated from the plots given in Figures 21 and 22 of the πp cross sections taken

from the open literature, and in particular from the recent compilation of Giacomelli, Pini, and Stagni.[31]

Most of the experimental points fall within the bounds of the calculation, and although the bounds are wide we must consider that the fit is remarkably good considering that all the available parameters in Yao's expression for the cross section (except for the relative phase of the two amplitudes) have been determined form other experiments. In particular, the agreement emphasizes the role played by the direct channel $T = 3/2$, Δ resonances in the πp system.

The one-pion-exchange model is only one of several quite different models that have been used in the interpretation of the process under consideration here. We have already alluded to the one-nucleon-exchange model in connection with the work of Heinz *et al.*[9] This has been reviewed by Brown.[32] The graph for this is given in Figure 20b. Such a graph can give no resonant structure because there are no poles occurring in the propagator in the physical region. According to Brown,[32] the one-nucleon-exchange graph gives a smooth behavior, much too large a

---

[31] G. Giacomelli, P. Pini, and S. Stagni, CERN/HERA 69-1.

[32] D. J. Brown, Nucl. Phys. *B7*, 37 (1968).

cross section, and too slow a fall off with energy. At 12 GeV/c the prediction is some 20 times larger than the experimental value. However, a part of the reaction amplitude must be due to such a graph, and it is a puzzle to understand what inhibitions operate to reduce its contributions to the much smaller level that it evidently obtains.

This question has been reconsidered by Uchiyama-Campbell and Silbar[33] who point out that the dnp-vertex involves an exchanged neutron leg which is rather far off-shell. For the measurements under consideration here, the momentum transfer, u, between the incoming proton and outgoing pion varies from about 0.3 $(GeV/c)^2$ down toward 0. Not much is known about the value of the vertex function for such small values of u. In view of this, a strong momentum dependence of the vertex function could drastically reduce the contribution of this graph. Moreover, absorption effects in the initial and final states can produce a further reduction. An attempt to impose absorption effects on the helicity amplitudes was carried out[33] and a significant reduction in the predicted cross sections was obtained. However, the result was still larger than the experiment, presumably because

---

[33]F. Uchiyama-Campbell and R. R. Silbar, Los Alamos Scientific Laboratory Report LA-DC-10315 (1969).

of the dubious treatment of the dnp-vertex.

One problem with the ONE graph is that it gives the wrong energy dependence. An improvement could be anticipated by Reggeizing the exchanged nucleon. A detailed discussion of the Reggeization in this case has been given by Lee.[34] Unfortunately, with Regge models usable formulas are obtained only in the asymptotic high energy limit. Here the theory gives an amplitude proportional to

$$\frac{1}{\Gamma(\alpha + \frac{1}{2})}\left[\frac{1 \pm e^{-i\pi(\alpha - \frac{1}{2})}}{\cos\pi\alpha}\right] s^{\alpha - \frac{1}{2}}$$

where $\pm$ is taken according to the signature of the trajectory. This leads to a differential cross section

$$\frac{d\sigma}{du} \sim s^{2\alpha(u)-2}.$$

First, consider a one-Regge-pole model with the exchanged nucleon the $N_\alpha(1/2^+(0.938), 5/2^+(1.688),----)$ trajectory with $T = 1/2$. For this trajectory, the usual assumption of linear dependence gives $\alpha = -0.38 + 1.0u$ so that for $u = 0$

$$\left(\frac{d\sigma}{du}\right)_{u=0} \sim s^{-2.76}.$$

---

[34] H. Lee, Phys. Rev. 174, 2130 (1968).

Furthermore, Barger and Michael[35] have pointed out that for this trajectory alone the amplitude has a zero at $\alpha = -1/2$, or at $u = -0.12$ (GeV/c)^2, well within the physical region. The experimental data of Allaby et al.[23] at 21.1 GeV/c shows no such pronounced dip. This fact is taken as evidence for the contribution of another trajectory, namely N_γ ($3/2^-(1.518)$, $7/2^-(2.190)$,----) with $\alpha = -0.8 + 1.0u$. Thus, the total amplitude should be a sum of two terms with zeros that do not coincide. In Regge language this situation is referred to as exchange degeneracy.[35] As noted by Barger and Michael, the exchange degenerate model is somewhat of an idealization since the N_α and N_γ trajectories are split apart. They constructed an "effective" trajectory between the two wrong-signature nonsense points $\alpha(N_\alpha) = -1/2$ and $\alpha(N_\gamma) = -3/2$ obtaining $\alpha_{eff} = -0.9 + 0.28u$. This effective trajectory yields a differential cross section $d\sigma/du$ for $u = 0$ which varies as $s^{-3.8}$.

To obtain a rough estimate of the experimental behavior we used the factor $\exp(-p_\perp/0.20)$ to extrapolate our differential cross sections above $E_{c.m.} = 3.9$ GeV and those of Allaby et al.[23] to give $d\sigma/du$ at $u = 0$. Such a procedure has questionable validity but we have, nevertheless, plotted the result in Figure 23 together with a least

---

[35] V. Barger and C. Michael, Phys. Rev. Letters 22, 1330 (1969).

squares fit to the data. These show a dependence

$$\left(\frac{d\sigma}{du}\right)_{u=0} \sim s^{-3.2}$$

a result somewhat in between the limits set by considering a single N_α trajectory or an "effective" trajectory.

Barger and Michael also considered the full kinematics[34] for Reggeization of reaction (1) using both N_α and N_γ trajectories and certain simplifying assumptions. By paramatizing the residues of the helicity amplitudes, they obtained a good fit to the high energy portion of the forward cross section as well as the 21.1 GeV/c angular distribution. However, these results required four otherwise undetermined parameters.

It is interesting to suggest that the three bumps in the forward cross section are due to direct channel dibaryon resonances according to the graph of Figure 20c. These fall on a linear rising trajectory as shown in Figure 24. The linear behavior follows from equation (3) which shows that if $M_\Delta^2 = s'$ has a linear behavior then $M_{pp}^2 = s$ will have one as well.

According to Graffi, Grecchi, and Turchetti,[36] the first peak may be the first Regge recurrence of the ^1S_o p-p pole (the unbound diproton) and arise from a $^1D_2$ resonance in the p-p system. Evidence for such a resonance has been

---

[36]S. Graffi, V. Grecchi, and G. Turchetti, Lett. Nuovo Cim. 2, 311 (1969).

Fig 23.--Plot of $d\sigma/du$ at $u = 0$ to show the s dependence above 7.1 GeV/c. The experimental data has been extrapolated to $u = 0$ using the factor $\exp(-p_\perp/0.20)$ as discussed in the text. The points near $s = 40$ GeV^2 are from Ref. 23.

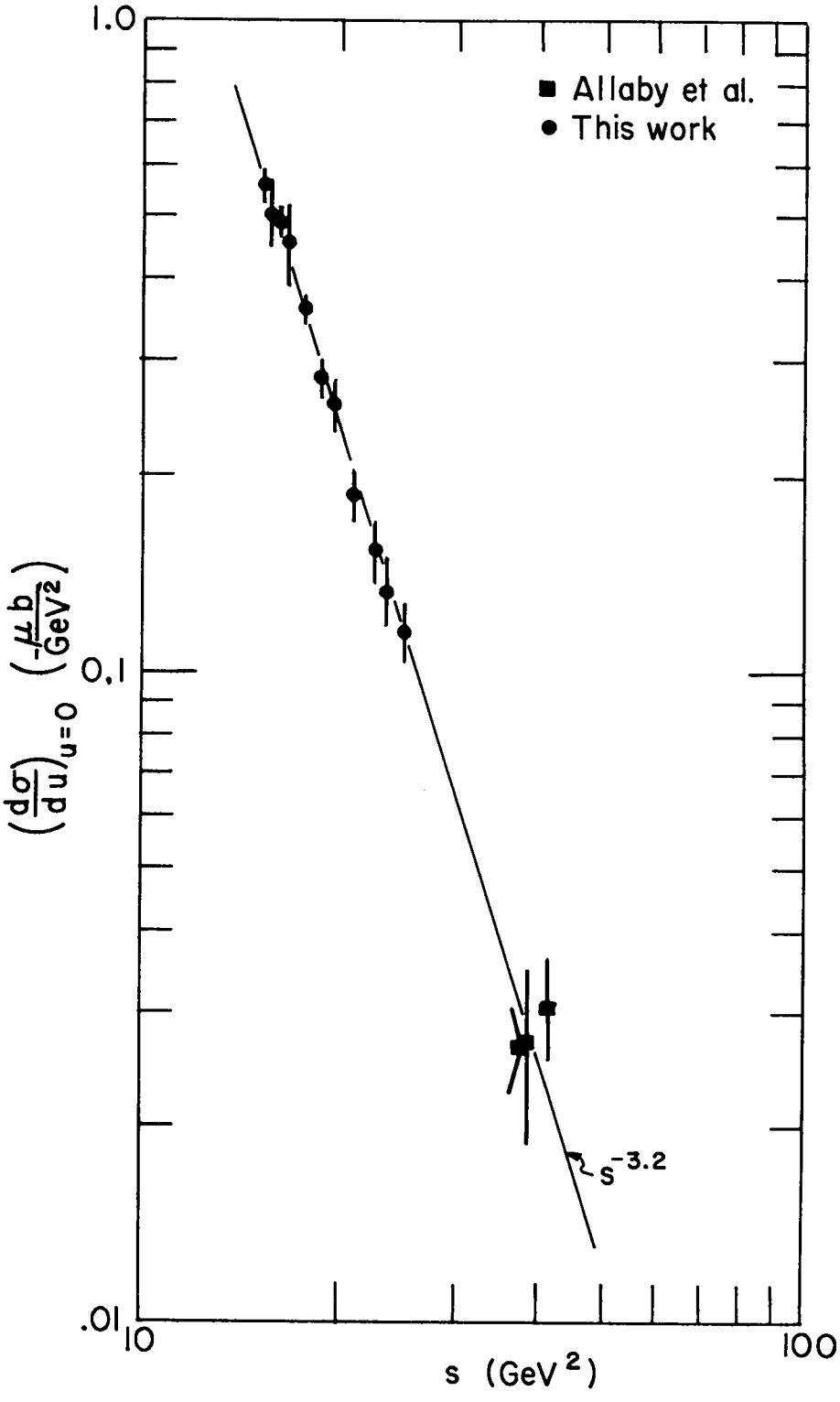
1.0
0.1
.01
10
100
■ Allaby et al.
● This work
$\left(\frac{d\sigma}{du}\right)_{u=0}$ $\left(\frac{\mu b}{GeV^2}\right)$
$\sim s^{-3.2}$
s (GeV^2)

Fig. 23.

Fig. 24.--Total c.m. energy squared of the p-p system ($s = M_{pp}^2$) versus the interger J suggesting a Regge trajectory for the dibaryon system. The data points are taken from the peaks appearing in the forward differential cross section for the reaction $p + p \rightarrow d + \pi^+$.

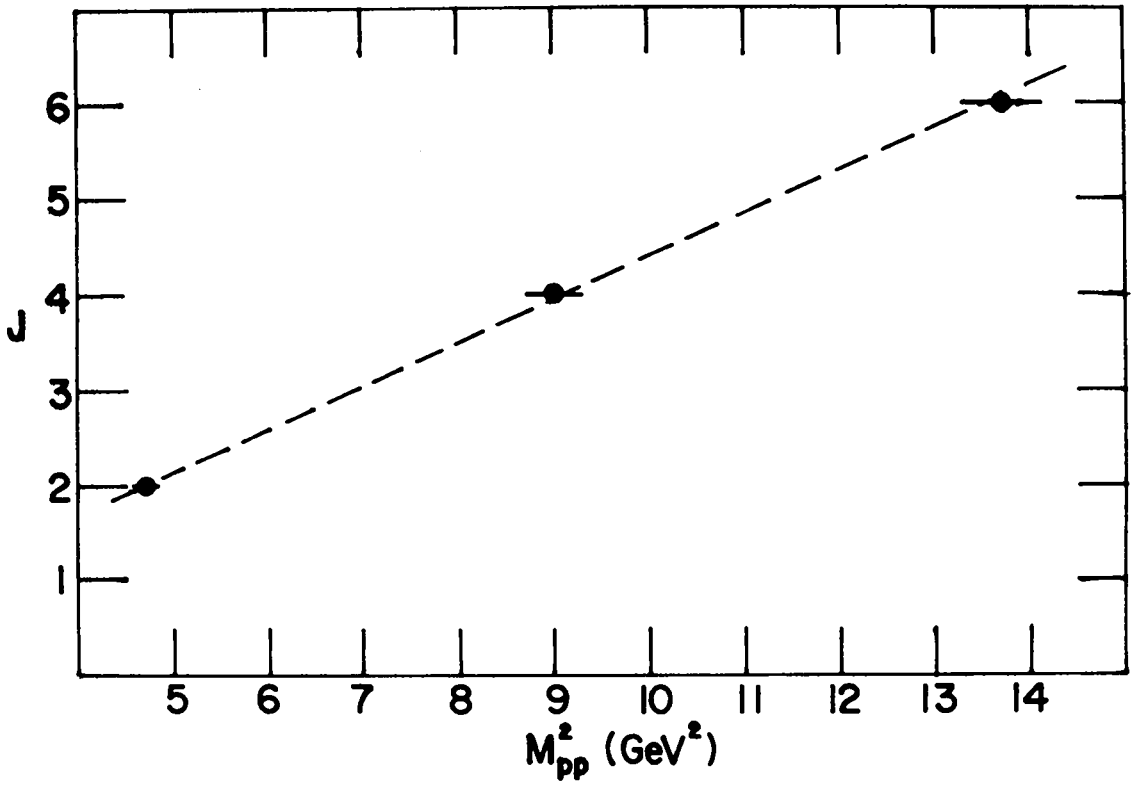

Fig. 24.

given by Arndt[37] based on a partial wave analysis of the elastic p-p scattering around 660 MeV.

However, the $^1D_2$ phase shifts are not very large and the argument that a pole exists in a non-physical region must be considered speculative at this stage. On the other hand, Mandelstam has argued that the strong resonant behavior of the $d\pi^+$ channel in this energy region could be explained in terms of an S-wave $\Delta_{3/2,3/2}p$ resonance with the same quantum numbers as $^1D_2$.

Following this idea the further bumps in our curve would correspond to further Regge recurrences at $M_{pp} = 3.0$ and 3.7 GeV with $J = 4$ and $J = 6$, respectively. A partial wave analysis based on careful measurements of the angular distribution in the energy region of the bumps might help decide the angular momentum character and parity of these states.

Other evidence for the existence of such a dibaryon trajectory has been reviewed by Libby and Predazzi[38] and supports the plausibility of this idea, but emphasizes the lack of good and convincing data.

The suggestion of dibaryon resonances is, of course, just one aspect of the larger subject of "exotic" resonances for which there is presently little evidence. However, if

---

[37] R. A. Arndt, Phys. Rev. 165, 1834 (1968).

[38] L. M. Libby and E. Predazzi, Lett. Nuovo Cim. 2, 881 (1969).

a duality principle[13] applies here, we should expect that s channel low energy resonances would follow naturally as an alternative description of the process of t an u channel Regge exchange.

In conclusion, this discussion brings out the primitive and ambiguous state of the theory of strong interaction processes. Surprisingly, in spite of its known inadequacies, especially in the description of high energy processes and those involving high momentum transfers, the one-pion-exchange mechanism offers the most satisfactory description of our data. The implication is that we are still far from the asymptotic limit for which simple Regge ideas can be expected to dominate.